



**Politecnico  
di Torino**

**Politecnico di Torino**

Master's Degree in Biomedical Engineering  
A.y. 2021/2022  
Graduation Session December 2022

# **Design and experimental test of a pulse oximeter system to acquire vital parameters**

Supervisors:

Prof. Alberto Vallan  
Prof. Jordi Cosp-Vilella

Candidate:

Catello Corso  
Matr. 289327

*Ai miei genitori  
e a zio Pino*

## Abstract

Photoplethysmography is spectrophotometric technique used to calculate vital parameters. It is a promising technology due to its simplicity, low cost, and non-invasiveness and it has the potential for early screening for various atherosclerotic and cardiac pathologies. Although this technology has been used in pulse oximetry for the past 40 years, much research and innovation are still related to this topic. This is due to the recent widespread use of wearable devices that constantly monitor vital parameters. Particularly in the last two years, the use of these devices has increased significantly, especially for home applications, due to the Covid-19 pandemic.

It is because of the growing interest in learning more about this technology and acquiring more knowledge about the world of biomedical instrumentation, which involves an inevitable combination of electronics and biomedicine, that this thesis project was born. It aims to develop a transmittance pulse oximetry device for calculating vital parameters such as pulse rate, arterial oxygen saturation, and pulse rate variability. Both the design part of the electronic circuit and the management and implementation of software algorithms to control the switching on of the LEDs and calculate the vital parameters are completely developed ex-Novo. The management of the circuit is handled via the Arduino Due board. A PCB was created for the designed circuit to facilitate the use of the device and reduce signal noise. Since it is often heard about telemedicine nowadays and how technology has made significant progress in this area, the idea arose to develop a web application that could be shared with the end-user (medical personnel) to allow real-time patient monitoring. The advantage of this option is that it facilitates the work of the doctor (e.g., in the case of a patient with covid) and of patients who perhaps have limited travel possibilities.

Finally, an experimental analysis is carried out, collecting data from twelve subjects (eight males and four females) and comparing them with a commercial pulse oximeter used as a reference. In addition to the analysis of measurement error, it is also shown how important health indices can be derived from a PPG signal, such as the relationship between large artery stiffness and age.





# Table of Contents

<b>List of Tables</b>	IV
<b>List of Figures</b>	V
<b>Acronyms</b>	VIII
<b>1 Motivation and scope of the project</b>	1
1.1 Motivation . . . . .	1
1.2 Objectives and scope of the project . . . . .	2
1.2.1 Objectives . . . . .	2
1.2.2 Scope of the project . . . . .	2
<b>2 Background</b>	3
2.1 Pulse oximetry: purposes and uses . . . . .	3
2.2 Basic principles and signal capture . . . . .	4
2.2.1 Basic principles . . . . .	4
2.2.2 Signal capture . . . . .	6
2.2.3 Lambert Beer's law . . . . .	7
2.3 Calculation of vital parameters . . . . .	9
2.3.1 SpO <sub>2</sub> : an estimation of arterial oxygen saturation . . . . .	9
2.3.2 Pulse rate (PR) and pulse rate variability (PRV) estimation	11
2.4 Limitations of pulse-oximetry . . . . .	13
<b>3 Analog front-end design and used materials</b>	14
3.1 Description of the project . . . . .	14
3.2 LED driving circuit . . . . .	15
3.2.1 Circuit diagram . . . . .	15
3.2.2 Timing for switching on LEDs . . . . .	17
3.3 Differential transimpedance amplifier stage . . . . .	19
3.3.1 Development of the circuit . . . . .	19
3.3.2 Design choices . . . . .	19

3.4	Probe manufacturing and circuit assembly . . . . .	22
<b>4</b>	<b>Signals acquisition and calculation of vital parameters</b>	<b>25</b>
4.1	PPG signals acquisition . . . . .	25
4.1.1	Timer Interrupt setting . . . . .	25
4.1.2	Setting the on/off cycle . . . . .	26
4.1.3	PPG signals visualization . . . . .	27
4.2	Calculation of vital parameters . . . . .	31
4.2.1	Algorithm for calculating PR . . . . .	33
4.2.2	Algorithms for calculating SpO <sub>2</sub> . . . . .	35
4.2.3	Algorithm for calculating PRV . . . . .	39
<b>5</b>	<b>Verification of the device and GUI design</b>	<b>41</b>
5.1	Verification and validation of device operation . . . . .	41
5.2	Matlab GUI design . . . . .	44
5.3	Development of Matlab Web App . . . . .	47
<b>6</b>	<b>Experimental tests and results</b>	<b>51</b>
6.1	Experimental tests on different subjects . . . . .	52
6.2	Discussion of the results . . . . .	76
6.3	Analysis of PPG waveform and large artery stiffness . . . . .	77
<b>7</b>	<b>Conclusions and Future Work</b>	<b>81</b>
<b>A</b>	<b>Electric scheme and PCB</b>	<b>84</b>
A.0.1	Electric scheme . . . . .	84
A.0.2	PCB manufacturing . . . . .	85
<b>B</b>	<b>MATLAB codes for vital parameters' algorithms</b>	<b>88</b>
B.0.1	Algorithm for PR calculation . . . . .	88
B.0.2	Algorithm 1 for SpO <sub>2</sub> calculation . . . . .	90
	<b>Bibliography</b>	<b>94</b>

# List of Tables

3.1	Initial specifications. . . . .	15
3.2	Operating conditions of ELM-4002 optical sensor. . . . .	16
3.3	Matching of digital I/O lines and buffer's pins. . . . .	17
3.4	Truth table for LED timing*. . . . .	17
4.1	GIMA OXY-2 specifications. . . . .	37
5.1	Comparison PR and SpO <sub>2</sub> values between the developed device and GIMA OXY-2 on 60-second of signal. . . . .	42
6.1	Subject 1 data*. . . . .	52
6.2	Subject 2 data. . . . .	54
6.3	Subject 3 data. . . . .	56
6.4	Subject 4 data. . . . .	58
6.5	Subject 5 data. . . . .	60
6.6	Subject 6 data. . . . .	62
6.7	Subject 7 data. . . . .	64
6.8	Subject 8 data. . . . .	66
6.9	Subject 9 data. . . . .	68
6.10	Subject 10 data. . . . .	70
6.11	Subject 11 data. . . . .	72
6.12	Subject 12 data. . . . .	74
6.13	Measurement errors. . . . .	76
6.14	SI values. . . . .	80

# List of Figures

2.1	Extinction coefficient for Hb and HbO <sub>2</sub> with respect to different wavelengths. ( <i>Source: [7]</i> ) . . . . .	5
2.2	Cross-sectional diagram of arteries and veins during cardiac cycle. ( <i>Source: [8]</i> ) . . . . .	6
2.3	Transmission vs reflective probes. ( <i>Source: [2]</i> ) . . . . .	7
2.4	Difference between absorbed and transmitted light through a biological tissue. ( <i>Source: [2]</i> ) . . . . .	8
2.5	Empirical calibration curve of a pulse oximeter - R values vs SpO <sub>2</sub> %. ( <i>Source: [10]</i> ) . . . . .	10
2.6	Typical waveform of a photoplethysmographic signal (PPG). ( <i>Source: [13]</i> ) . . . . .	11
2.7	ECG and PPG waveform and related inter-beat-intervals. ( <i>Source: [15]</i> ) . . . . .	12
3.1	Hardware block diagram. . . . .	15
3.2	LEDs driving circuit. . . . .	16
3.3	Example of timing for LEDs switching ON/OFF. . . . .	18
3.4	Differential current sensing transimpedance configuration. . . . .	19
3.5	Waveform of the output signal. . . . .	20
3.6	Components incorporated in the probe. . . . .	22
3.7	Manufactured probe. . . . .	22
3.8	Circuit mounted on breadboard. . . . .	23
3.9	Final PCB. . . . .	24
4.1	Flowchart of Arduino code for switching on/off cycle. . . . .	27
4.2	Raw signals with Configuration 1. . . . .	28
4.3	Raw signals with Configuration 2. . . . .	28
4.4	Raw signals with Configuration 3. . . . .	29
4.5	Raw signals with Configuration 4. . . . .	29
4.6	Raw signals with Configuration 5. . . . .	30
4.7	Raw signals with Configuration 6. . . . .	30

4.8	PPG raw signals. . . . .	32
4.9	PPG filtered signals. . . . .	32
4.10	PPG intervals. ( <i>Source: [11]</i> ) . . . . .	33
4.11	Flowchart of the algorithm for calculating PR. . . . .	34
4.12	Flowchart of the algorithm 1 for calculating SpO <sub>2</sub> . . . . .	36
4.13	Calibration line for Algorithm 1. . . . .	38
4.14	Calibration line for Algorithm 2. . . . .	38
4.15	Flowchart of the algorithm for calculating PRV. . . . .	40
5.1	Comparison of PR measurments. . . . .	43
5.2	Comparison of SpO <sub>2</sub> measurments. . . . .	43
5.3	Visualization of the Graphical User Interface. . . . .	45
5.4	Representation of the text file with patient's informations. . . . .	46
5.5	Software block diagram . . . . .	47
5.6	MATLAB Web App Server configuration. . . . .	48
5.7	Visualization of the web app on <i>Google Chrome</i> browser. . . . .	49
5.8	Web app operation. . . . .	50
6.1	Subject 1 parameters' comparison. . . . .	53
6.2	Subject 2 parameters' comparison. . . . .	55
6.3	Subject 3 parameters' comparison. . . . .	57
6.4	Subject 4 parameters' comparison. . . . .	59
6.5	Subject 5 parameters' comparison. . . . .	61
6.6	Subject 6 parameters' comparison. . . . .	63
6.7	Subject 7 parameters' comparison. . . . .	65
6.8	Subject 8 parameters' comparison. . . . .	67
6.9	Subject 9 parameters' comparison. . . . .	69
6.10	Subject 10 parameters' comparison. . . . .	71
6.11	Subject 11 parameters' comparison. . . . .	73
6.12	Subject 12 parameters' comparison. . . . .	75
6.13	PPG signal of subject 8. . . . .	78
6.14	PPG signal of subject 11. . . . .	79
6.15	PPG signal of subject 12. . . . .	79
A.1	Electric scheme. . . . .	84
A.2	PCB design in EasyEDA. [Scale 1:1] . . . . .	85
A.3	Top Layer of PCB design. [Scale 1:1] . . . . .	86
A.4	Bottom Layer of PCB design. [Scale 1:1] . . . . .	86
A.5	Step 1-2 of PCB manufacturing. . . . .	87
A.6	Step 3-4 of PCB manufacturing. . . . .	87



# Acronyms

**Hb** Reduced Hemoglobin

**HbO2** Oxygenated Hemoglobin

**SaO2** Functional arterial oxygen saturation

**SpO2** Estimation of arterial oxygen saturation

**PR** Pulse Rate

**PRV** Pulse Rate Variability

**HRV** Heart Rate Variability

**IBI** Inter-Beats-Interval

**PPG** Photoplethysmographic signal

**ADC** Analog to Digital Converter

**GUI** Graphical User Interface

**PCB** Printed Circuit on Board

**GND** Ground

**IP** Internet Protocol

**DVP** Digital Volume Pulse

**PWV** Pulse Wave Velocity

# Chapter 1

## Motivation and scope of the project

### 1.1 Motivation

The idea of this project arises from previous work done during the "*Wearable Devices*" course led by prof. Jordi Cosp-Vilella.

In the last two years, the whole world has come up against one of the most challenging times in history in the previous century, the SARS-CoV-2 pandemic, which counts more than 426,000,000 infections and about 6,000,000 deaths all over the world[1]. Although SARS-CoV-2 is considered a systemic disease, it attacks mainly the lungs leaving permanent marks on the infected and, in some cases causing the infected to die. The first action taken to monitor the possible aggravation of this disease is the measurement of blood oxygen saturation. It is known that oxygen is very vital for the proper functioning of each cell in the human body, and oxygen level in blood can be an important indicator of health [2]. This has led to the wide use of pulse oximeters that are easy to use at home where monitoring is needed.

The actuality of this device and its importance in the biomedical field have been the critical points for increasing interest in the subject and developing a device for calculating vital parameters while also allowing telemonitoring through the development of a web app.



## 1.2 Objectives and scope of the project

### 1.2.1 Objectives

The main objectives of the thesis are briefly summarized below:

- Design and development of an analog front-end for a finger transmission pulse oximeter
- Acquisition of vital parameters as: arterial oxygen saturation ( $\text{SpO}_2$ ), pulse rate (PR), pulse-rate variability (PRV)
- GUI to display the signal, its parameters and the patient's information
- Development of a Web App to share with other users allowing the telemonitoring of a subject
- Statistical analysis and comparison of vital parameters in different subjects

### 1.2.2 Scope of the project

This thesis project aims at designing and developing an analog front-end for a finger transmission pulse oximeter. In addition to the analog electronics aspect, it also deals with developing appropriate algorithms for device operation and the calculation of vital parameters related to the captured photoplethysmography signal. The software used for the algorithms is *Arduino IDE* for signal handling and acquisition, while *MATLAB* is used for calculating vital parameters. After testing and verifying the device's functioning, a GUI that represents the signal, its parameters, and the information of the subjects is progressed. The development of the GUI in *MATLAB* is linked to the subsequent evolution of a Web App, which can be shared with other users, enabling the result of a possible telemonitoring for the patient. Finally, experimental tests on different subjects are carried out to validate the device's functioning.

The development of such a device will be helpful to have an experimental platform for future students of the *Wearable Devices* course to practice their knowledge in electronics and possibly expand the project improving it.

# Chapter 2

## Background

### 2.1 Pulse oximetry: purposes and uses

Pulse oximetry is a common and non-invasive method used for monitoring arterial blood oxygen saturation ( $\text{SpO}_2$ ) and pulse rate of human heart. By acquiring these important vital parameters, doctors can monitor the health status of patients suffering from pulmonary diseases or other clinical conditions involving a decrease in oxygen saturation. For example, some conditions that can be monitored are [3]:

- Chronic obstructive pulmonary disease
- Asthma
- Pneumonia
- Lung cancer
- Anemia
- Cardiac arrest
- Congenital heart disease

In addition to what is mentioned above, pulse oximetry also plays a key role in surgical operations involving anesthesia. During surgeries the patient's cardiopulmonary system is placed in a state where it can no longer meet oxygen demands on its own [2]. This causes the need for an anesthesiologist to track and control the patient's vitals which includes the arterial oxygen saturation. This is known to be one of the variables that provides instant feedback with regards to the patient's status. The non-invasive nature, fast response, and affordability of the pulse oximetry has made it indispensable during clinical anesthesia [4].

Arterial oxygen saturation values normally range from 95% to 100% in healthy people, while values <90% could quickly lead to an aggravation of the state and values below 70% are life threatening [5].

## 2.2 Basic principles and signal capture

### 2.2.1 Basic principles

Pulse oximetry involves the use of a light source where normally a light emitted by a LED passes through a given biological tissue while a photodetector measures the amount of light passing through the tissues (bones, skin, etc.) or reflected by them.

This is a spectrophotometric technique that is based on two physical principles: i) the different absorption spectra of oxyhemoglobin ( $\text{HbO}_2$ ) and reduced hemoglobin (Hb); ii) the presence of a pulsatile signal found in the arteries being relatively independent from non-pulsatile signal [6].

Hemoglobins such as  $\text{HbO}_2$  and Hb that are able to bind reversibly with molecular oxygen are called functional hemoglobins [2]. When comparing the amount of  $\text{HbO}_2$  with respect to the sum of oxygenated and reduced hemoglobin in arterial blood, the functional arterial oxygen saturation ( $\text{SaO}_2$ ) can be obtained through the following equation:

$$\text{FunctionalSaO}_2 = \frac{Hb}{Hb + HbO_2} \cdot 100\% = \frac{c_{Hb}}{c_{HbO_2}} \cdot 100\% \quad (2.1)$$

where,  $c_{Hb}$  and  $c_{HbO_2}$  represent the concentration of oxygenated hemoglobin and reduced hemoglobin in arterial blood.

The arterial oxygen saturation calculated through a pulse oximeter is defined as  $\text{SpO}_2$ . It differs from the functional  $\text{SaO}_2$ , which is measured by a gaseous invasive-blood method.

In arterial blood also dysfunctional hemoglobins are present. Oppositely to the previously described hemoglobins, dysfunctional ones do not bind with molecular oxygen and so they do not provide its transport to the tissues. The four most common dysfunctional hemoglobins are: methemoglobin (MetHb), carboxyhemoglobin (COHb), sulfhemoglobin, and carboxysulfhemoglobin [2]. These hemoglobins also absorb light as functional hemoglobins do.

While  $\text{SaO}_2$  allows to calculate the fractional oxygen saturation of arterial blood (percentage of the amount of oxygenated hemoglobin with respect to the sum of all hemoglobins), with pulse oximetry it is not possible. Nevertheless, since functional hemoglobins are the main light absorbers, the error in calculating an estimation of the arterial oxygen saturation ( $\text{SpO}_2$ ) through a pulse oximeter is less than 3% with respect to  $\text{SaO}_2$ .

As mentioned earlier, the key feature of the functional hemoglobins is the different way they absorb light which depends on the wavelengths they are exposed to. By looking at *fig. 2.1*, it can be seen how Hb and HbO<sub>2</sub> have significant differences in the absorption of red and infrared light wavelengths.

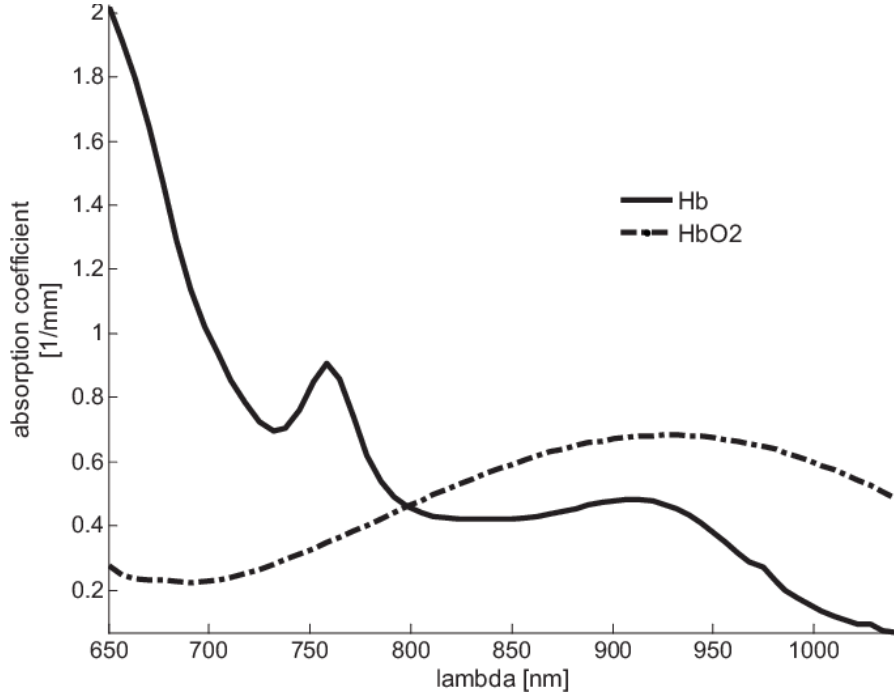


**Figure 2.1:** Extinction coefficient for Hb and HbO<sub>2</sub> with respect to different wavelengths. (*Source: [7]*)

Red and infrared light wavelengths penetrate tissues easily whereas blue, green, yellow, and far-IR lights are significantly absorbed by the nonvascular tissues and water [8].

When comparing the light absorption of oxygenated hemoglobin and reduced hemoglobin, it can be seen in the *fig. 2.1* that HbO<sub>2</sub> absorbs more IR light than Hb, while Hb absorbs more red light than HbO<sub>2</sub>. For this reason, well-oxygenated blood with its higher concentrations of HbO<sub>2</sub> appears bright red to the eye since it scatters more red light when compared to Hb. On the other hand, Hb absorbs more red light and appears to have a reduced brightness of red [8].

In addition to the different absorption spectra of hemoglobin, pulse oximetry is able to calculate the arterial oxygen saturation SpO<sub>2</sub> thanks to the variation of the amount of red and infrared light absorbed within the cardiac cycle. The segment of light that is transmitted through arteries tissues generates signals that have two components: i) non-pulsatile (DC) due to the diastole of the cardiac cycle; ii) pulsatile (AC) due to the systole.

*Fig. 2.2* shows a cross-sectional diagram of an artery and a vein during systole and diastole. It illustrates the non-pulsatile (DC) and pulsatile (AC) compartments of arteries and the relative absence of volume change in veins and capillaries [8].

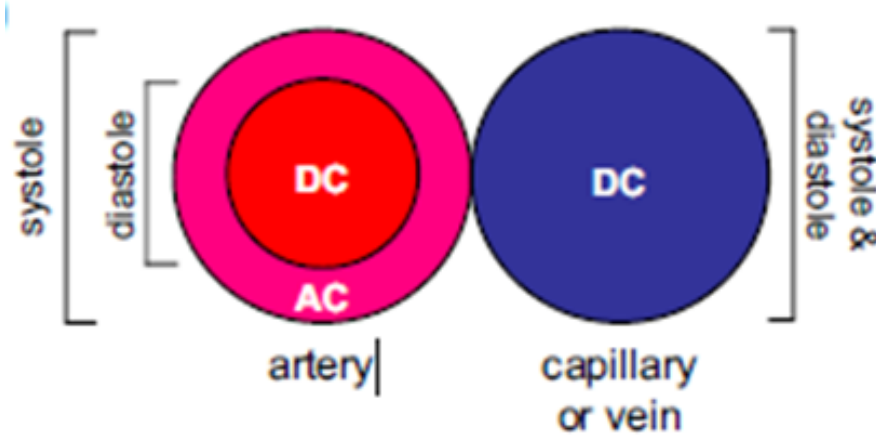


**Figure 2.2:** Cross-sectional diagram of arteries and veins during cardiac cycle. (Source: [8])

### 2.2.2 Signal capture

Exploiting the difference in light absorption properties between  $\text{HbO}_2$  and  $\text{Hb}$  and tracking the change in light absorbance as the blood pulses, most pulse oximeters emit two wavelengths of light (red at 660nm and near-IR at 940nm) from a pair of small LEDs [8]. The choice of these two wavelengths is because the extinction coefficients of  $\text{Hb}$  and  $\text{HbO}_2$  vary as much as possible. Another issue for the wavelength choice is the flatness of the absorption spectra shown in *fig. 2.1* around the chosen wavelengths [2].

The light emitted from LEDs passes through tissues (or it is reflected by them) and it is captured by a photodetector that produces current linearly proportional to the intensity of light striking it. Usually, LEDs and photodetector are packed in a probe.

According to the position of LEDs and photodetector in the probe, two types of pulse oximeters exist: i) a transmission pulse oximeter that measures the amount of light passing through the tissue and so, transmitted to the photodetector; ii) a reflectance pulse oximeter that measures the amount of light reflected to the probe.

On one hand, transmission pulse oximeters are mostly used in body tissues that are usually thin and allow the transmittance of light, i.e., fingers, ears, toes. In these probes the LEDs and the photodetector are placed opposite each other in

a clip. On the other hand, reflectance pulse oximeters present the LEDs and the photodetector on the same side of the probe. They are mostly used for wearable devices, able to detect vital parameters also during physical activity. A widespread application of reflective sensors is in wrist-worn watches for monitoring the wrist's pulse. *Fig. 2.3* shows the arrangement of LEDs and photodetector for the two described cases.

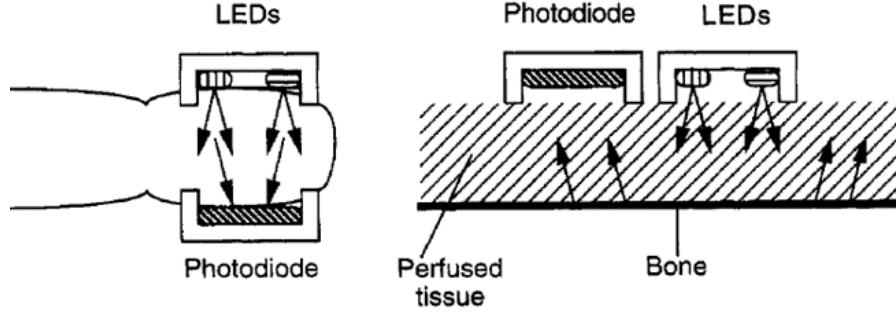


**Figure 2.3:** Transmission vs reflective probes. (*Source: [2]*)

### 2.2.3 Lambert Beer's law

The theoretical background to the attenuation of light through human tissue is given by Lambert-Beer's law. It describes mathematically the attenuation of light travelling through a uniform medium containing an absorbing substance [2].

Lambert-Beer's law states that when a monochromatic incident light, which intensity is  $I_0$ , enters a medium, a part of the light is transmitted through it and another part is absorbed. The intensity of the transmitted light is given by:

$$I = I_0 \cdot e^{-\epsilon(\lambda)cd} \quad (2.2)$$

where  $\epsilon(\lambda)$  is the extinction coefficient of the absorbing substance at a specific wavelength  $\lambda$ ,  $c$  is the concentration of the absorbing substance which is constant in the medium and  $d$  is the geometric path length through the medium.

The transmittance of light travelling through a medium that absorbs a portion of light is represented by the ratio of the transmitted light ( $I$ ) on the incident light ( $I_0$ ). Since in a biological tissue, as a finger, there are many components that can absorb light such as bones, skin pigmentation and blood, the total absorbance is defined as:

$$A_t = \sum_{i=1}^N \epsilon_i(\lambda) c_i d_i \quad (2.3)$$

where  $n$  represents the number of the different  $i$ -absorbing substances.

According to the 2.3 and to the fact that arteries contain more blood during systole than diastole (see *fig. 2.2*) it is possible to state that: the absorbance of light in tissues with arteries increases during systole mainly because of the larger quantity of absorbing substances in blood such as hemoglobin [2]. Indeed, when arteries undergo a systolic event, the geometrical path  $d$  in the arteries increases due to the dilatation of the vessel. This alternating part of the total absorbance allows to differentiate between a constant component in absorbance (non-pulsatile DC component) and a varying component due to the pulsatile behaviour of arterial blood (AC component).

The time varying signal captured by the photodiode is denoted as the plethysmographic (or photoplethysmographic) signal [2]. *Fig. 2.4* shows the difference between absorbed and transmitted light through a biological tissue. Particularly, during a cardiac cycle, the intensity of light passing (transmitted) through the tissue during diastole ( $I_H$ ) is higher with respect to the systolic event ( $I_L$ ). This is because during systole also the AC component of arterial blood is present.

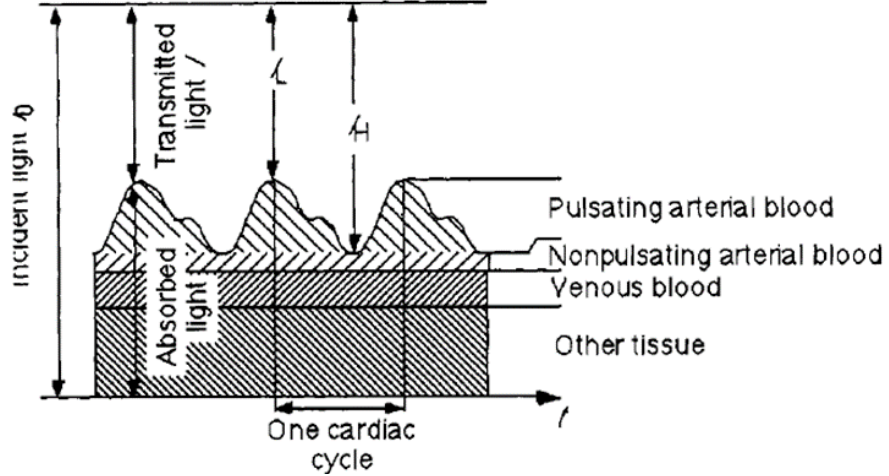


**Figure 2.4:** Difference between absorbed and transmitted light through a biological tissue. (*Source: [2]*)

The intensities of transmitted lights  $I_H$  and  $I_L$ , respectively related to diastolic and systolic events, are:

$$I_H = I_0 \cdot e^{-\epsilon_{DC}(\lambda)c_{DC}d_{DC}} \cdot e^{-(\epsilon_{Hb}c_{Hb} + \epsilon_{HbO2}c_{HbO2}) \cdot d_{min}} \quad (2.4)$$

$$I_L = I_0 \cdot e^{-\epsilon_{DC}(\lambda)c_{DC}d_{DC}} \cdot e^{-(\epsilon_{Hb}c_{Hb} + \epsilon_{HbO2}c_{HbO2}) \cdot d_{max}} \quad (2.5)$$

In the equations 2.5-2.4 the components  $\epsilon_{DC}$ ,  $c_{DC}$ ,  $d_{DC}$  are termed as DC components and they represent the constant absorbers present during the diastole

and systole (for example bones, skin, muscles, etc.). The DC components are equal for both the transmitted light intensities and they are independent from arterial blood. Instead, the absorbing components related to the arterial blood change according to the diameter's dilatation of arterial vessel. Particularly there is a minimum diameter during diastole and a maximum diameter during systolic arterial dilatation.

## 2.3 Calculation of vital parameters

### 2.3.1 SpO<sub>2</sub>: an estimation of arterial oxygen saturation

Pulse oximeters use the amplitude of the absorbances at the two different wavelengths to compute an estimation of the arterial oxygen saturation (SpO<sub>2</sub>). The parameter calculated to obtain the SpO<sub>2</sub> is the modulation ratio of the absorbances of red and infrared lights [8].

In order to overcome the non-linearities in the transmitted signals due to LEDs, photodetector and light absorbance in the tissues, the transmitted light signals of the red and infrared light are normalized with respect to the maximum intensity of light transmitted during diastole ( $I_H$ ) for each wavelength [2]. This computation results in having two signals with the same intensities of the DC components. The only difference between the signals is the AC component, which reflects the changes in the transmitted light related to blood pulsation in arteries. The modulation ratio  $R$  can be defined as the ratio of the total absorbances:

$$R = \frac{A_{t,R}}{A_{t,IR}} \quad (2.6)$$

where the total absorbances of red ( $A_{t,R}$ ) and infrared light ( $A_{t,IR}$ ) are respectively:

$$A_{t,R} = \ln \frac{I_{L,R}}{I_{H,R}} \quad (2.7)$$

$$A_{t,IR} = \ln \frac{I_{L,IR}}{I_{H,IR}} \quad (2.8)$$

In conclusion it can be stated that the modulation ratio  $R$  is the ratio between the pulsatile and the non-pulsatile light components for each wavelength:

$$R = \frac{\overline{AC_R}}{\overline{DC_R}} \cdot \frac{\overline{DC_{IR}}}{\overline{AC_{IR}}} \quad (2.9)$$



Once the modulation ratio has been calculated, it is necessary to find a relationship between  $R$  and  $SpO_2$ . In fact, although Lambert-Beer's Law well explains the physiological processes underlying pulse oximetry, it must be considered that not all the light emitted by LEDs is absorbed or transmitted through tissues. A portion of the incident light is scattered and thus deviated from its initial path. For this reason, the amount of absorbed light is greater than the effective. This occurs when photons are refracted by an object of their similar size and there is a change in the index of refraction at the interface of this object. In this case, red and infrared light's wavelength has the same order of magnitude of the diameter of red blood cells ( $7\mu m$ ) [2].

It is therefore necessary to develop an empirical calibration curve. The most used methods involve analysing healthy human volunteers by recording values of arterial oxygen saturation corresponding to different  $R$  values, by means of a CO-oximeter or other prototypes [9]. In a controlled desaturation study, test subjects breathe a sequence of gas mixtures of decreasing oxygen content while connected to the prototype monitor [10]. So, an accurate table of appropriate  $R$  values related to  $SpO_2$  is built. An example of an empirically determined calibration curve is shown in *fig. 2.5*.

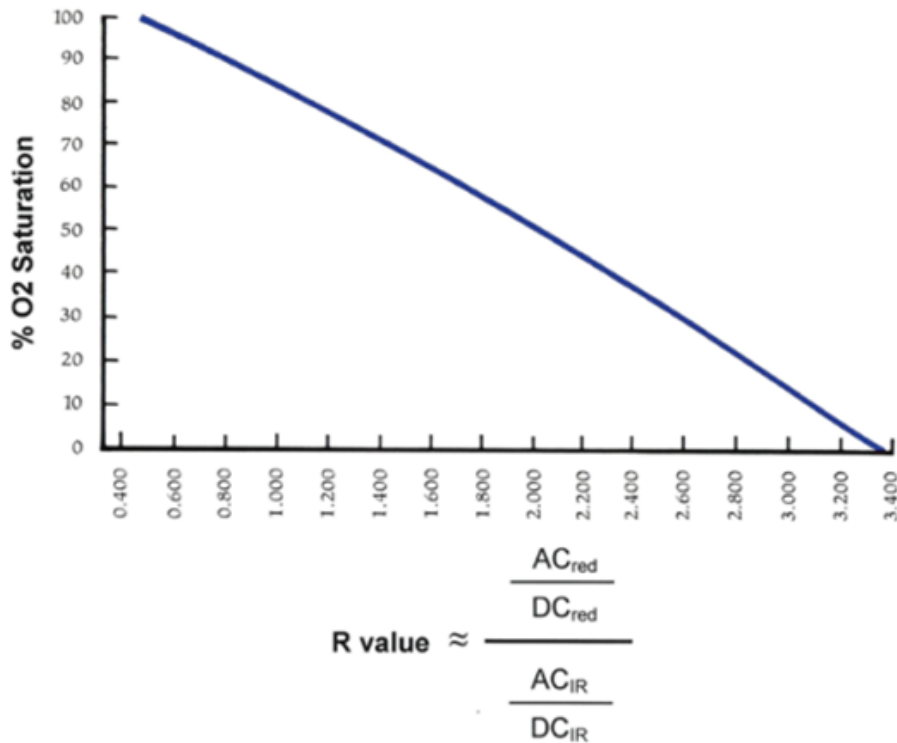


**Figure 2.5:** Empirical calibration curve of a pulse oximeter -  $R$  values vs  $SpO_2\%$ . (Source: [10])

Usually test subjects are desaturated until 75-80%, that is the medical threshold to avoid permanent complications in human health. Thus, the R-value lookup table in every pulse oximeter is empirically calibrated only within some survivable range of  $\text{SpO}_2$  but becomes less accurate at low values [9].

### 2.3.2 Pulse rate (PR) and pulse rate variability (PRV) estimation

Fig. 2.6 describes the typical photoplethysmographic signal (PPG) obtained by the transmitted light of one of the two LEDs which hits the photodiode. The shape of the PPG pulse is commonly divided into two phases: the anacrotic phase is the rising edge of the pulse, whereas the catacrotic phase is the falling edge of the pulse [11]. The first phase represents the systolic peak, and the second phase the diastolic one. A dicrotic notch, shown in the figure, is usually seen in the catacrotic phase of subjects with healthy compliant arteries [11]. The dicrotic notch corresponds to a small increase in aortic pressure that occurs immediately after the end of cardiac systole, at the closure of the aortic semilunar valve [12].

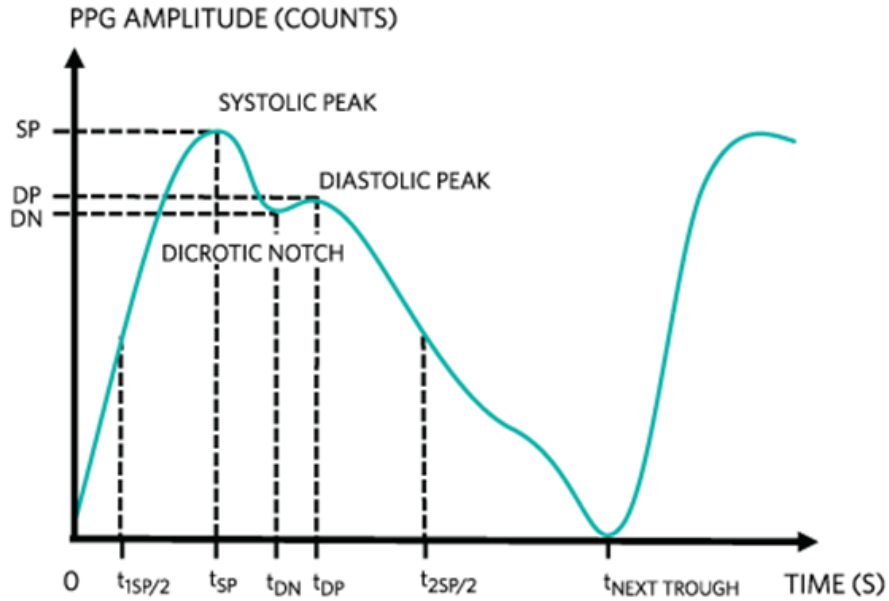


**Figure 2.6:** Typical waveform of a photoplethysmographic signal (PPG). (Source: [13])

Since each systolic peak represents a heartbeat, the number of peaks during 60s of recorded signal will be the heart rate (HR) expressed in beat-per-minutes (bpm). PR can be easily estimated, knowing the time difference (inter-beats-interval = IBI) between two subsequent peaks, as follows:

$$PR = \frac{60}{IBI[s]}[bpm] \quad (2.10)$$

In addition to PR, another important parameter for monitoring the health status of a subject is the heart rate variability (HRV). HRV is the fluctuation in the time intervals between adjacent heartbeats [14]. HRV indexes neurocardiac function and is generated by interactions between heart and brain and dynamic non-linear autonomic nervous system processes. An optimal level of HRV is associated with health and self-regulatory capacity, and adaptability or resilience [14]. Usually, HRV is measured through an ECG. An estimation of HRV is the pulse rate variability (PRV) that can be obtained from a PPG signal.

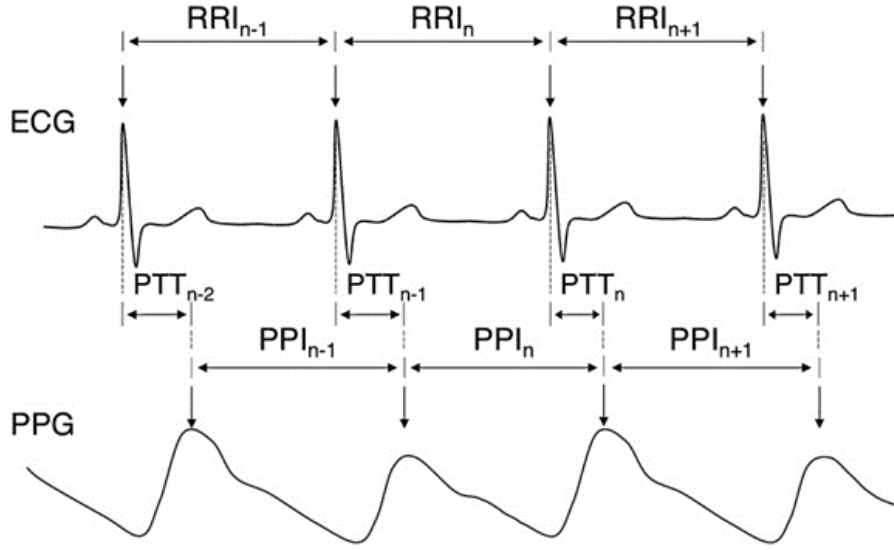


**Figure 2.7:** ECG and PPG waveform and related inter-beat-intervals. (*Source: [15]*)

*Fig. 2.7* shows the difference between IBI in ECG and PPG signals. Particularly, for the PPG signal there is a shift in time respect to the R peak of the ECG signal, denoted a pulse transit time (PTT). The pulse transit time refers to the time needed for a pulse wave to travel between two arterial sites (in pulse oximetry specifically is the time to travel from the heart to the place where measurement is done, such as the finger) [16].

## 2.4 Limitations of pulse-oximetry

Since pulse oximeters do not require user calibration, they have some limitations that may give false readings. These devices will function properly only with a correct detection of the modulation in transmitted light. If perfusion is lower and pulse amplitude is small, the signal amplitude will be decreased, and the device will be liable to error [17].

Low-amplitude signal tracings may be due to poor tissue perfusion resulting from vasoconstriction and/or hypotension. The main causes include distributive or hypovolemic shock, hypothermia, use of vasoconstrictor agents, and poor cardiac output due to pump failure or dysrhythmia [8].

Motion artifacts can interfere with signal detection and interpretation of the PPG waveform. Improperly placed sensors, shivering, seizures, or parkinsonian tremors can cause movement, creating an inaccurate reading [17].

Another factor that can affect  $\text{SpO}_2$  readings is the presence of abnormal levels of hemoglobin. Because pulse oximeters are based only on two wavelength readings, they cannot distinguish between oxygenated hemoglobin and carboxyhemoglobin (COHb) [2]. Therefore, increased levels of COHb will cause an overestimation in  $\text{SpO}_2$ . According to this, smokers will often have artificially high readings after smoking a cigarette [17].

Some environmental factors can also lead to errors in  $\text{SpO}_2$  readings, such as: cold rooms, bright light or sunshine, electrical interferences, and nail polish [17].

## Chapter 3

# Analog front-end design and used materials

### 3.1 Description of the project

As seen in the introductory chapter, in order to develop an effective pulse oximetry device capable of calculating  $\text{SpO}_2$  and other vital parameters, it is necessary to use at least two LEDs with different emission wavelengths.

In particular, in this project a dual drive optical sensor with two wavelengths at 660nm and 940nm (red and infrared light) is used. The ELM-4000 series emitter assemblies are sensors specially designed for medical applications where selection of peak wavelength is a key requirement [18].

Another fundamental component in the construction of the pulse oximeter probe is the photodetector. In this case, a BPW34, a silicon PIN photodiode is used. It is characterised by high speed and high radiant sensitivity [19].

The photodiode and the optical sensor are connected to an Arduino Due microcontroller board based on an Atmel SAM3X8E ARM Cortex-M3 CPU. The board receives a 5V ( $\pm 5\%$ ) power supply via a PC USB port. Three tri-state buffers packed in a quadrupole buffer (CD74HC126E) with tri-state output are used to drive the alternating red and infrared light LEDs. The three buffers are supplied with 3.3V via Arduino and are driven by the six digital I/O lines "22-27".

As for the photodiode, its output is fed into a differential transimpedance amplifier stage consisting of three OpAmps packed into a quad operational amplifier (TLC274IN). The quad operational amplifiers are supplied with 5V via Arduino board.

Finally, the output of the differential transimpedance amplifier stage is input to the pin A0 of the ADC of the SAM3X8E ARM Cortex-M3 microcontroller. The ADC is set on 12 bits (4096 levels). *Fig. 3.1* shows the block diagram of the

hardware for the analog front end of the device.

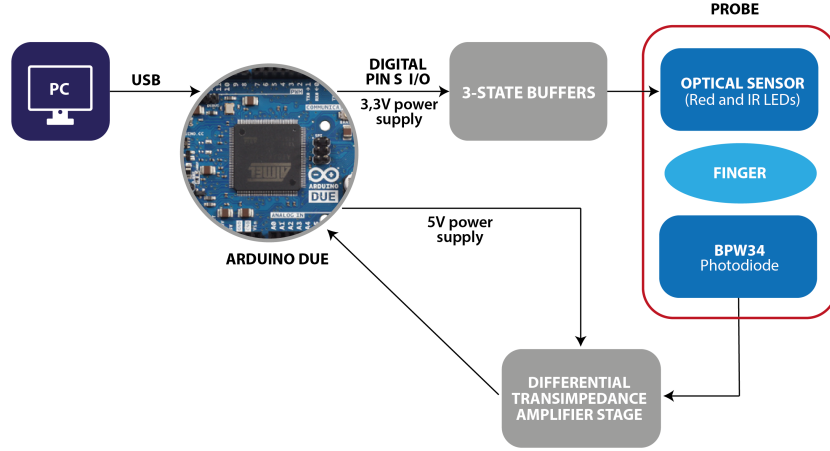


**Figure 3.1:** Hardware block diagram.

The Table 3.1 summarizes all the initial specifications of the project:

Specification	Value
Power supply for Arduino Due	5V( $\pm 5\%$ ) via USB
Power supply for tri-state buffer	3.3V via Arduino
Power supply for quadropole OpAmp	5V via Arduino
Frequency of the internal timer clock 2 of microcontroller	42 MHz
Timer Interrupt	66.67 $\mu$ s
Voltage measurement interval	6.67 ms
ADC resolution	12 bits

**Table 3.1:** Inital specifications.

## 3.2 LED driving circuit and timing

### 3.2.1 Circuit diagram

Three tri-state buffers are used to alternatively drive the two LEDs in the optical sensor. In particular, an analysis of the ELM-4002 optical sensor datasheet shows that the adequate operating conditions of the two LEDs are the following:

Wavelength	If	Vf
660nm	20 mA	1.85 V
940nm	20 mA	1.20 V

**Table 3.2:** Operating conditions of ELM-4002 optical sensor.

To comply with the operating specifications, considering that the quadrupole tri-state buffer (CD74HC126E) receives a 3.3V power supply from the Arduino Due board and using the first Ohm's law, we obtain that:

$$R_{660} = \frac{V_{al} - V_f}{I_f} = \frac{(3.3 - 1.85)[V]}{20[mA]} = 72.5\Omega \quad (3.1)$$

$$R_{940} = \frac{V_{al} - V_f}{I_f} = \frac{(3.3 - 1.20)[V]}{20[mA]} = 105\Omega \quad (3.2)$$

According to equations 3.1 and 3.2, two resistors with nominal values of  $33\Omega$  ( $\pm 5\%$ ) and  $68\Omega$  ( $\pm 5\%$ ) respectively are chosen. This is because when the Red LED is ON, current flows only through the  $68\Omega$  resistor, while when the Infrared LED is ON, current flows through both resistors, as seen in the figure below.

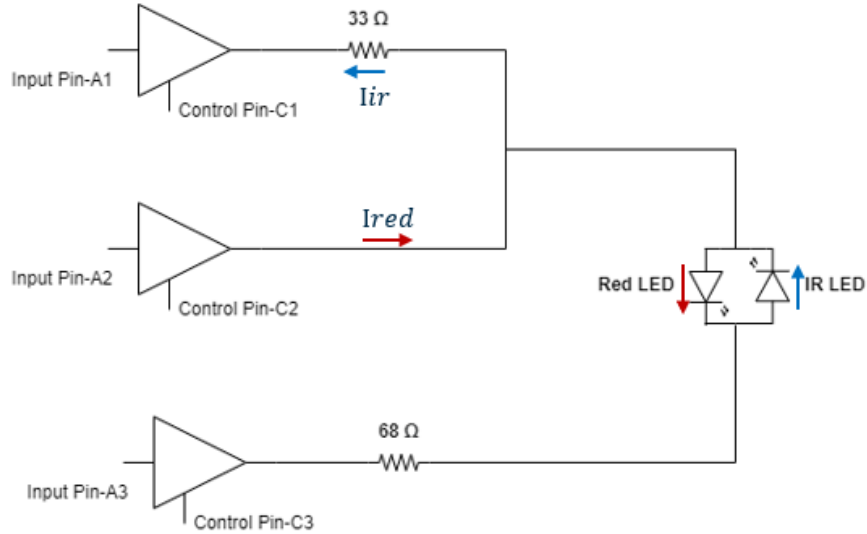


**Figure 3.2:** LEDs driving circuit.

In this case, there will be a current  $I_{660}$  of approximately 21.3 mA and a current  $I_{940}$  of 20.8 mA, which satisfies the above-mentioned operating specifications.

### 3.2.2 Timing for switching on LEDs

The two LEDs are alternately driven and switched on through six digital I/O lines of the Arduino board. The cycle of switching the LEDs on and off involves three phases: 1) both LEDs are OFF; 2) only the Red LED is ON; 3) only the Infrared LED is ON.

During the first phase, where none of the LEDs is ON, the ambient light component ( $V_{amb}$ ) is acquired through the analog pin A0 of the ADC. So, it is possible to cancel out the error in the PPG signal due to ambient light simply subtracting  $V_{amb}$  from the values acquired by the pin A0 when red ( $V_R$ ) and infrared ( $V_{IR}$ ) components are acquired.

The tri-state buffers' input and control pins are connected to the Arduino digital I/O lines "22-27". Notably, according to *fig. 3.2*, the relationship between the digital lines and the buffers pin is represented by the following table:

Buffer PIN	Digital I/O PIN
A1	22
C1	23
A2	24
C2	25
A3	26
C3	27

**Table 3.3:** Matching of digital I/O lines and buffer's pins.

By appropriately programming the input and control pins of each buffer, a truth table for LEDs timing management can be obtained.

A1	C1	A2	C2	A3	C3	LED state
L	H	L	H	L	H	OFF
L	L	H	H	L	H	RED-ON
L	H	L	L	H	H	IR-ON

**Table 3.4:** Truth table for LED timing\*.

\* Notice: H-> High logical level / L -> Low logical level.

The duration of a whole LEDs on/off cycle is 20 ms, appropriately divided for each phase. The sampling frequency results to be 50Hz. *Fig. 3.3* represents an



example of timing for LEDs switching on/off, where a value at the input of A0 for each state of the LEDs is acquired about every 6.67 ms.

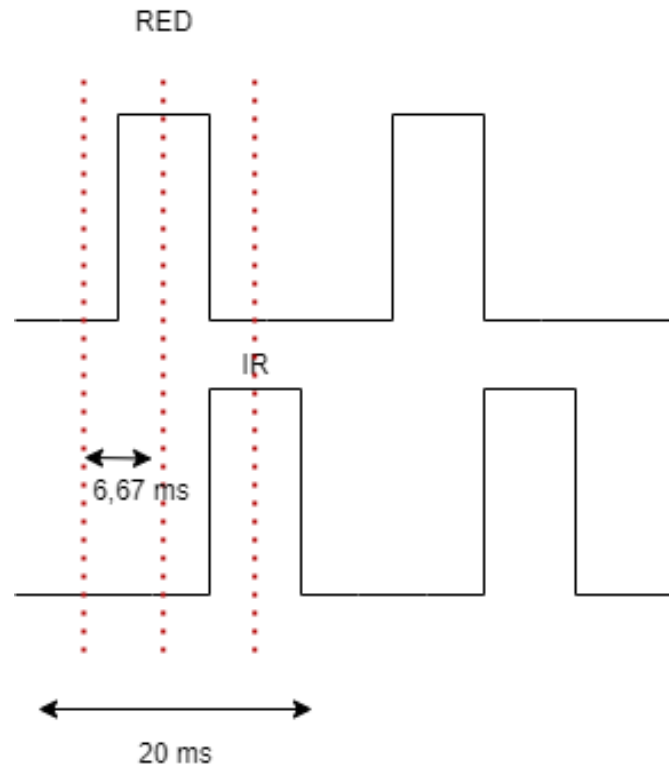


**Figure 3.3:** Example of timing for LEDs switching ON/OFF.

### 3.3 Differential transimpedance amplifier stage

#### 3.3.1 Development of the circuit

Since the photodiode signal of interest is a current, it is necessary converting it into a voltage signal. For this reason, a transimpedance amplifier stage is used. Notably, the current  $I_p$ , flowing through the photodiode, can drive two different inputs in a differential fashion, as seen in *fig. 3.4*. Since this current flows in different directions for the two amplifiers in the differential configuration, this will result in an output voltage twice as high as in a single-ended stage.

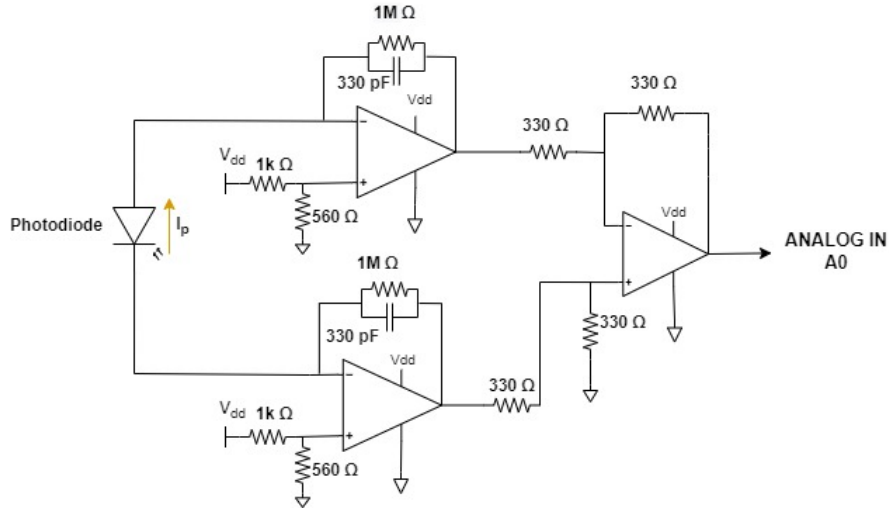


**Figure 3.4:** Differential current sensing transimpedance configuration.

Remarkably, the output voltage in input to the A0 channel of the ADC converter of Arduino results to be  $2 * I_p * R_f$ , where  $R_f$  are the feedback resistors of the first two amplifiers.

An advantage of this configuration is the common-mode rejection of coupled noise. By feeding the output of the current-to-voltage conversion into a differential amplifier stage, the noise will show up as a common mode signal on both inputs and have a canceling effect at output [2].

#### 3.3.2 Design choices

Concerning the choice of the feedback components used to develop the differential transimpedance amplifier stage, some considerations must be made.

Firstly, by analyzing the circuit in *fig. 3.4*, it is evident that the feedback resistors ( $R_f$ ) and capacitors ( $C_f$ ) form a low-pass filter for both the OpAmp where

the current  $I_p$  flows to the feedback components. The values of the feedback components are essential for setting both the cut-off frequency of the filters and the  $RC$  time constant.

The choice of a low cut-off frequency can result in high  $RC$  constants that may lead to errors in signals acquisition. Particularly, the low-pass filter  $RC$  time constant should have sufficiently high bandwidth (as shown in *equation 3.3*) because the input current consists of pulses [20].

$$R_f \cdot C_f \leq \frac{\text{Sample time}}{10} \quad (3.3)$$

In this case, the sample time is 20 ms for each cycle of switching on/off of the LEDs.

Therefore, for these considerations, the  $R_f$  and  $C_f$  values chosen are  $1\text{M}\Omega$  and  $330\text{pF}$ . This will result in a one-pole low-pass filter cut-off frequency of approximately  $482\text{Hz}$  and a  $RC$  time constant of  $330\mu\text{s}$ .

*Fig. 3.5* shows the waveform of the output signal to the third OpAmp (i.e., the input signal to the ADC) obtained with the oscilloscope, when the finger is inserted into the probe. By looking at it, some other considerations arise.

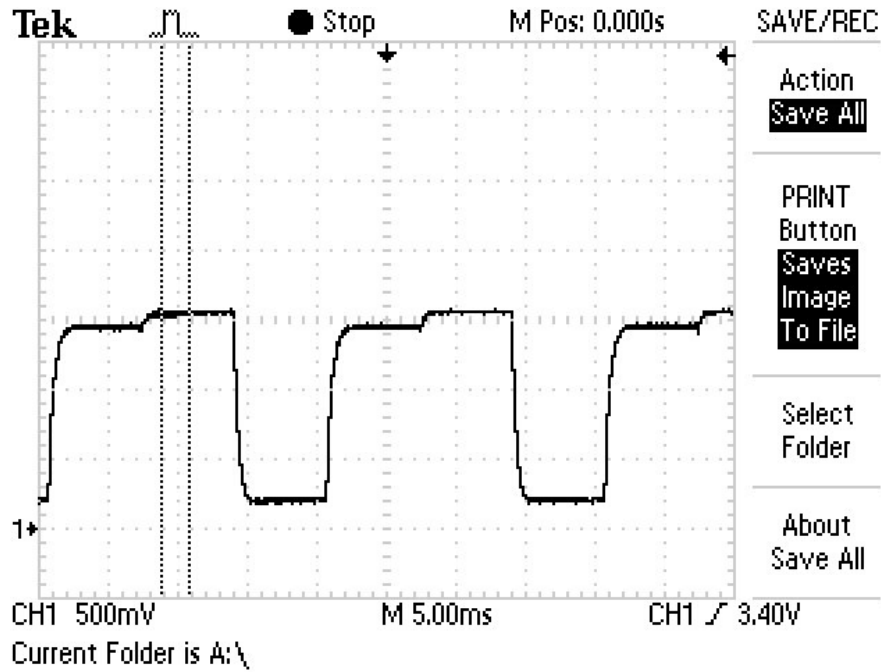


**Figure 3.5:** Waveform of the output signal.

It is possible to distinguish the three different phases of the switching cycle. The first phase, when both LEDs are OFF, is represented by the lowest step. Instead,

the step representing the Red LED signal is the one with the lower height of the remaining two. Indeed, Red light is much more absorbed than IR by human tissues.

Moreover, it is better to acquire each of the values ( $V_{\text{amvb}} - V_{\text{R}} - V_{\text{IR}}$ ) after the transient is exhausted in order to minimize errors in the acquisition. Catching the signal in the middle of each plateau, i.e. 3.33 ms after the transient, will result in a negligible error, less than 0.01% as can be derived from eq. 3.4:

$$\varepsilon = 1 - e^{-\frac{\Delta t}{\tau}} \quad (3.4)$$

being,  $\tau = 330 \mu\text{s}$  and  $\Delta t = 3.33 \text{ ms}$ .

A further aspect that needs to be underlined is the saturation of the OpAmp. As expressed in the datasheet of the TLC274IN component, it correctly works with input voltages in the range of  $0 \div 4.20 \text{ V}$ . Therefore, to avoid having negative input voltages at the upper OpAmp, it is reasonable to set the non-inverting inputs of both amplifiers to a reference voltage  $V_{\text{ref}}$ . This voltage should be chosen not too high to avoid saturation of the second OpAmp.

After careful measurements with the multimeter, a  $V_{\text{ref}}$  of 1.80 V is chosen. A voltage divider consisting of two resistors of  $1\text{k}\Omega$  and  $560\Omega$  generates the above-mentioned voltage at the non-inverting inputs of the two OpAmp.

### 3.4 Probe manufacturing and circuit assembly

The laboratory technicians have fabricated the probe incorporating the photodiode and the dual-wavelength LED. The components used are shown in *fig. 3.6*.

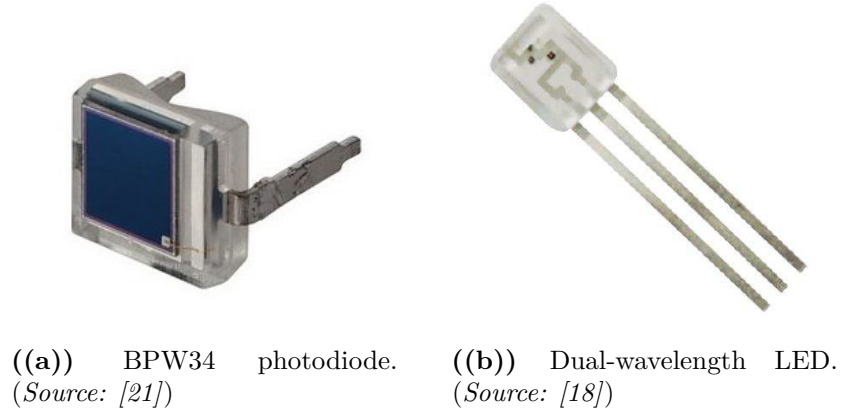


**Figure 3.6:** Components incorporated in the probe.

*SolidWorks* design software is used to design the shape of the probe, which is manufactured with a 3-D printer. *Fig. 3.7* illustrates the manufactured probe.

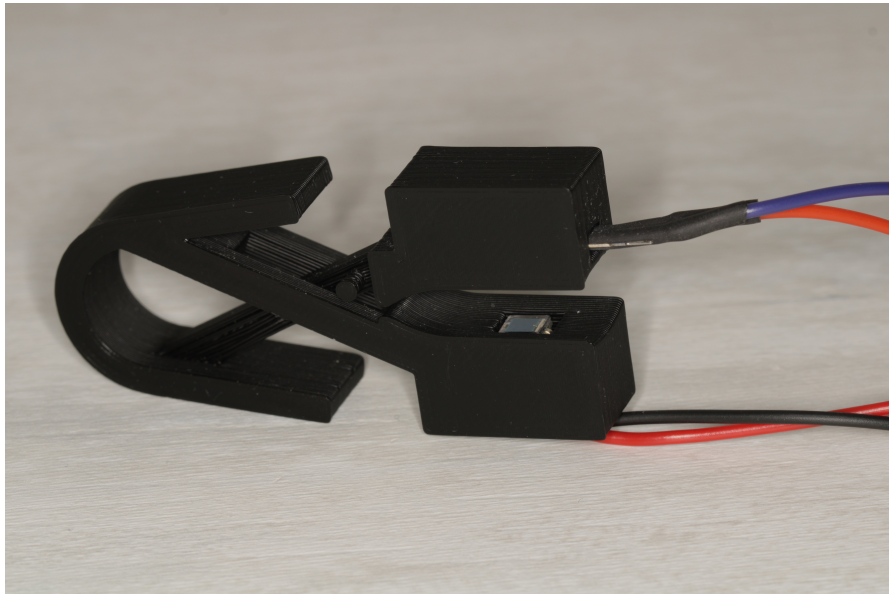


**Figure 3.7:** Manufactured probe.

The four connection cables shown in *fig. 3.7* represent respectively:

- Red → Anode of the photodiode
- Black → Cathode of the photodiode
- Orange → pin 1 of the LED
- Violet → pin 2 of the LED

After fabricating the probe, the circuit is mounted on an electronic breadboard following the electric scheme reported in Appendix A. An example of the final mounted circuit and its connections with Arduino board is depicted in the below figure.

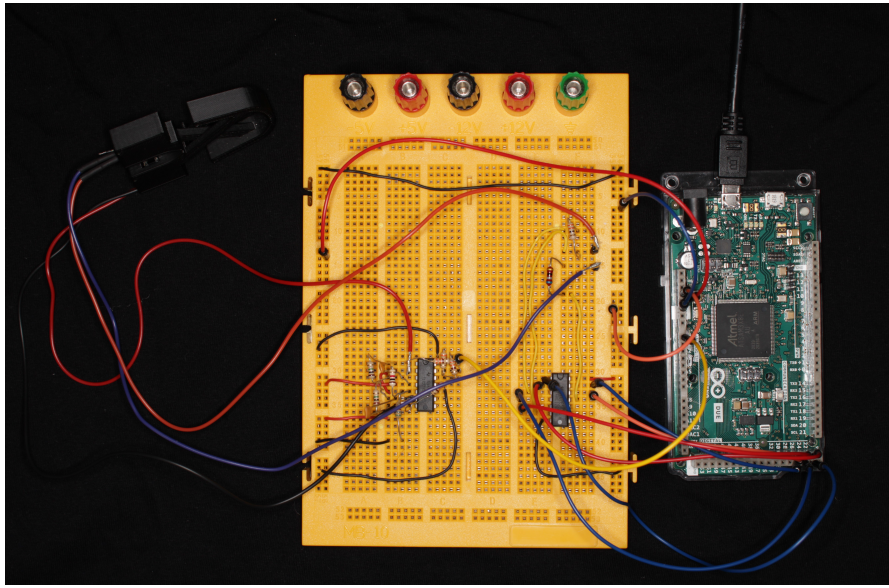


**Figure 3.8:** Circuit mounted on breadboard.

Since the circuit mounted on the breadboard can be cumbersome or subject to more noise due to inefficient connections, it is advisable designing a PCB. Appendix A illustrates the design of the circuit to be printed and the processes for manufacturing the PCB. The final circuit obtained is shown in *fig. 3.9*.

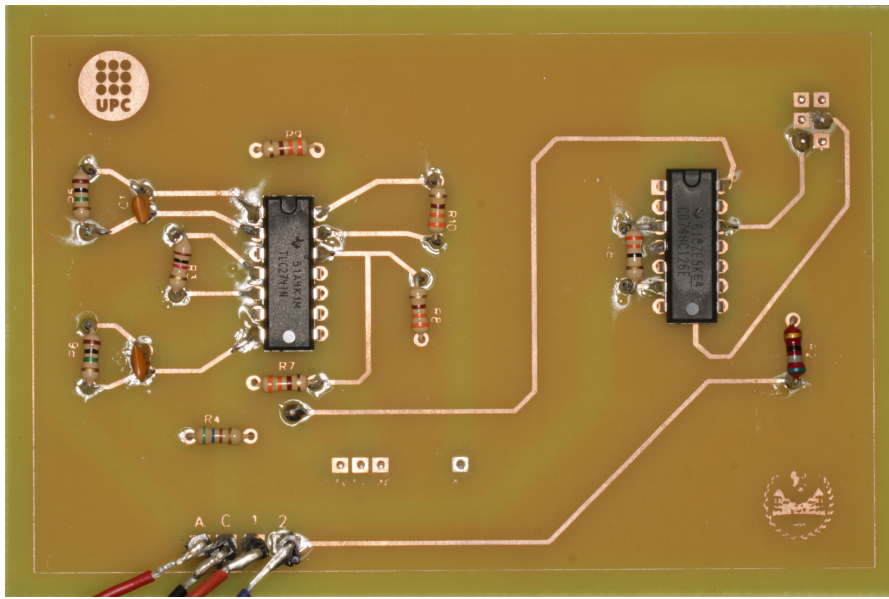


**Figure 3.9:** Final PCB.

Thanks to the connectors soldered on the PCB pads, the board can be easily inserted into the appropriate pins of Arduino. This results in greater precision in signal acquisition and improved device usability.

## Chapter 4

# Signals acquisition and calculation of vital parameters

The first part of this chapter deals with the acquisition of samples and the display of photoplethysmographic signals (PPG) obtained from the two different LEDs. The codes for managing the on/off cycle of the LEDs, the Timer Interrupt, and the representation of the signals are described in the first part.

Instead, the second part of the chapter outlines and analyzes the algorithms used to calculate vital parameters.

### 4.1 PPG signals acquisition

#### 4.1.1 Timer Interrupt setting

As expressed in the section 1.2.1 the *Arduino IDE* software manages the LED on/off cycle and acquires the output signal to the ADC via the analog pin A0.

A  $66.67\mu\text{s}$  interrupt timer handles the timing of signal acquisition and LED switching. In order to set the timer interrupt, it is necessary to study and analyze the datasheet of the Cortex-M3 microcontroller.

The first operation is enabling the clock inputs to many of the peripherals and the Cortex-M3 Processor. This is done through the Power Management Controller (PMC), which optimizes power consumption by controlling all system and peripheral user clocks. After that, the timer clock, the waveform mode, and the waveform selection are set through the register TC\_CMR (Timer Counter-Channel Mode Register). Mainly is selected the Timer Clock 1 (it divides by two the Master Clock Controller, set at 84MHz), and UP mode with the automatic trigger on RC



Compare. From the selected settings, TC2 channel two is activated. Then the value assigned to the trigger threshold TC\_RC sets the frequency of each timer interrupt. The frequency value is given by  $(MCK/2)/TC\_RC$  [Hz]. The following lines represent a sketch of the code.

```
void tc_setup() {

    PMC->PMC_PCER1 |= PMC_PCER1_PID35; // TC8 power ON : Timer Counter 2
                                         // channel 2 IS TC8

    TC2->TC_CHANNEL[2].TC_CMR = TC_CMR_TCCLKS_TIMER_CLOCK1
    // MCK/2 = 42 M Hz, clk on rising edge
                                | TC_CMR_WAVE           // Waveform mode
                                | TC_CMR_WAVSEL_UP_RC;
    // UP mode with automatic trigger on RC Compare

    TC2->TC_CHANNEL[2].TC_RC = 2800;
    //<***** Frequency = (Mck/2)/TC_RC Hz

    TC2->TC_CHANNEL[2].TC_IER = TC_IER_CPCS; // Interrupt on RC compare match
    NVIC_EnableIRQ(TC8_IRQn);
    TC2->TC_CHANNEL[2].TC_CCR = TC_CCR_SWTRG | TC_CCR_CLKEN;
    // Software trigger TC2 counter and enable
}
```

#### 4.1.2 Setting the on/off cycle

As described above in section 3.2.2, there are three phases during the cycle of switching the LEDs on and off. A 'Counter' variable is set, which is incremented to the desired value at each timer interrupt to select the duration of the entire cycle. In this case, the first phase calculates the value of  $V_{amb}$  when both LEDs are off. In the next two steps, alternately, the  $V_R$  and  $V_{IR}$  values related to the switching on of the two LEDs are calculated. In this way, the ambient light cancellation is obtained by subtracting  $V_{amb}$  from  $V_R$  and  $V_{IR}$ . Using a control variable "flag", the end of a cycle is established and thus the acquisition with subsequent plotting of the signals due to red and infrared light. The baud rate for the serial communication between Arduino and the PC is 115200 bps. The flowchart of the code for the switching on/off cycle management is represented in the *fig. 4.1*.

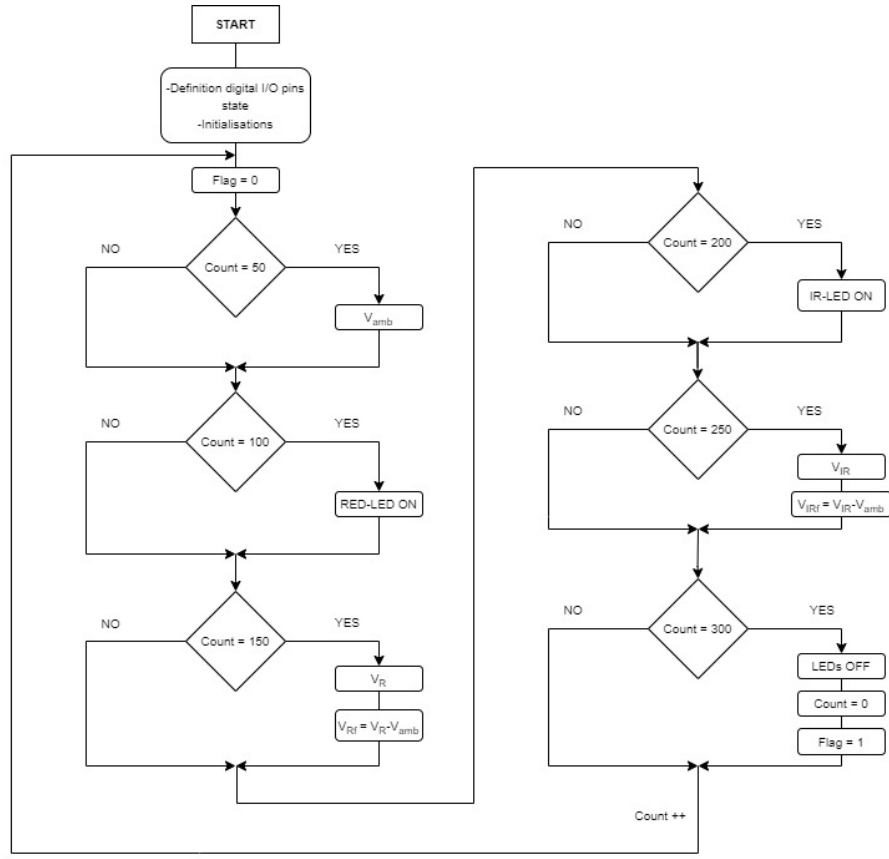


**Figure 4.1:** Flowchart of Arduino code for switching on/off cycle.

This flowchart represents the case where only one sample is acquired for each phase. It is also possible to have a sample average, acquiring more samples for each plateau by simply modifying the code.

### 4.1.3 PPG signals visualization

As it can be seen from the flowchart of *fig. 4.1*, when the variable "flag" differs from zero, it means that a cycle has finished, and so the acquired samples can be plotted and visualized in the *Serial Plotter* of *Arduino IDE*.

Several configuration are tested to choose the one that gives the most precise and least noisy raw PPG signals. The changing parameters related to each configurations are: the sampling frequency for an entire cycle, the number of samples averaged in every phase. The duration of the timer interrupts ( $66.67 \mu s$ ), the resolution of the ADC (12 bits) and the Baud Rate (115200 bps) are kept constant for every configuration. The different configurations tested will be shown below.

- **Configuration 1**

- Sampling Frequency = 30 Hz;
- Samples Average per phase = 1;

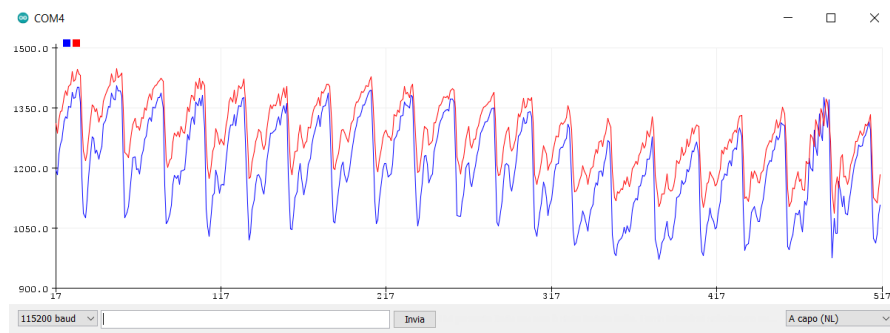


**Figure 4.2:** Raw signals with Configuration 1.

- **Configuration 2**

- Sampling Frequency = 30 Hz;
- Samples Average per phase = 3;

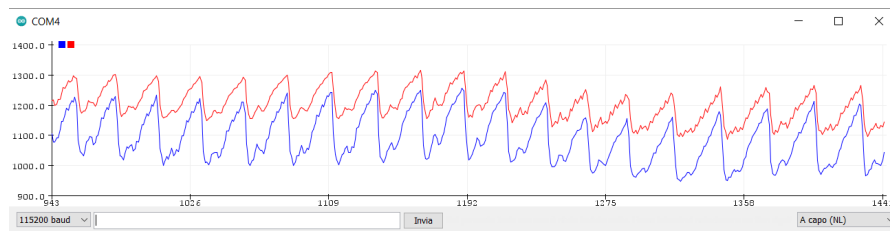


**Figure 4.3:** Raw signals with Configuration 2.

- **Configuration 3**
  - Sampling Frequency = 50 Hz;
  - Samples Average per phase = 1;

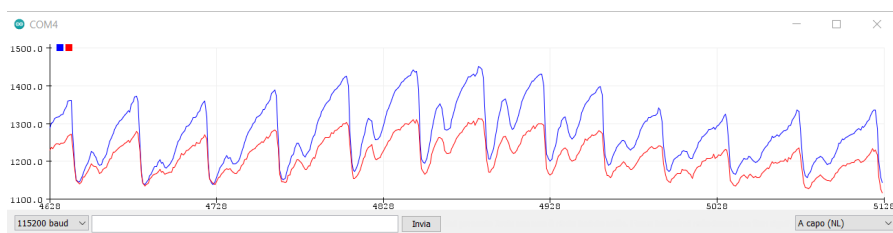


**Figure 4.4:** Raw signals with Configuration 3.

- **Configuration 4**
  - Sampling Frequency = 50 Hz;
  - Samples Average per phase = 3;

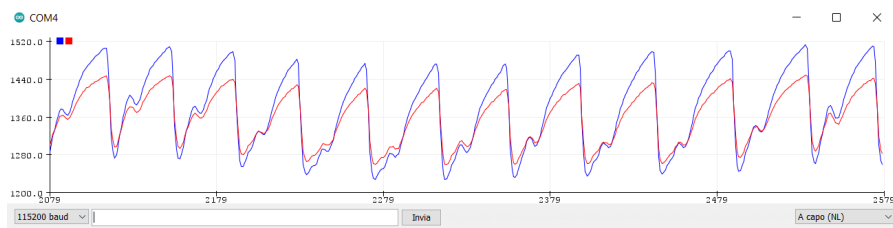


**Figure 4.5:** Raw signals with Configuration 4.

- **Configuration 5**

- Sampling Frequency = 100 Hz;
- Samples Average per phase = 3;

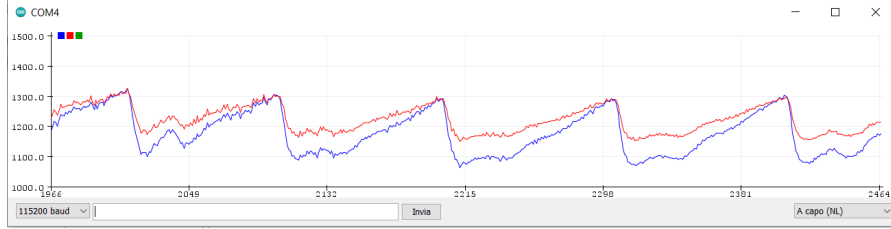


**Figure 4.6:** Raw signals with Configuration 5.

- **Configuration 6**

- Sampling Frequency = 50 Hz;
- Samples Average per phase = 10;

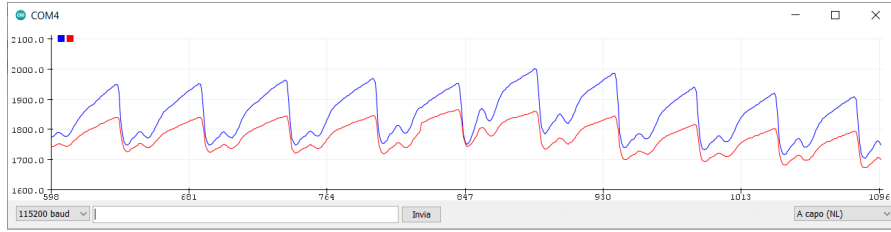


**Figure 4.7:** Raw signals with Configuration 6.

For all the depicted configuration the x-axes represents the number of the samples, while the y-axes is the amplitude of the PPG signals according to the  $2^{12}-1$  levels of the ADC.

All tests are performed on the same person and under same ambient light conditions. The raw signals captured are related to the right index finger.

By analyzing the different configurations, it can be stated that the most are the samples averaged, and the best is the visualization of the raw signals. According to the previous figures (4.2-4.7), the best configurations that give the less noisy raw signals are the 4th and the 6th. The configuration with a sampling frequency per cycle of 100Hz results in being too noisy as the 1st one. The 2nd and the 3rd seem better but still not the other two.

For this reason, the 6th configuration is selected to carry out the device calibration tests and calculate vital parameters.

## 4.2 Calculation of vital parameters

After correctly acquiring the signal, the next step is to develop the algorithms to calculate vital parameters such as pulse rate (PR), arterial oxygen saturation ( $\text{SpO}_2$ ), and pulse rate variability (PRV).

These algorithms are implemented in MATLAB and provide the calculation of vital parameters in real-time during acquisition. Indeed, it is possible to establish serial communication between MATLAB and Arduino via the COM 4 Serial Port (USB port used to connect Arduino to the PC).

The PPG signal may be filtered to eliminate irrelevant frequency content, such as high-frequency noise or low-frequency baseline wander as shown for example in *fig. 4.2* and *4.3*. High-frequency noise can be eliminated using a low-pass filter. A low-pass cutoff frequency as low as 2.25 Hz may be suitable for PR estimation, whereas higher cutoff frequencies are required for analyses of pulse wave timing (such as 5 Hz for interbeat interval (IBI) calculation) [22]. Low-frequency baseline wander can be eliminated using a high-pass filter. A suitable high-pass cut-off frequency can be 0.4 Hz, ensuring that even the lowest plausible PR of 30 bpm is preserved [22].

For the above considerations, the signals are filtered through 250-sample-long recursive windows with an IIR digital Butterworth bandpass filter. The passband is between 0.4 and 10 Hz. Throughout these windows (250 samples  $\rightarrow$  approx. 5s), the vital parameters are calculated and averaged according to the number of peaks detected in the PPG signals.

An example of a recording of about 35 seconds of the two PPG signals is reported. *Fig. 4.8* depicts the raw PPG signals, while *fig. 4.9* shows the two PPG signals after being filtered. It is evident, comparing the two figures, the baseline wander in the non-filtered signals and how it is deleted, filtering out the DC component.

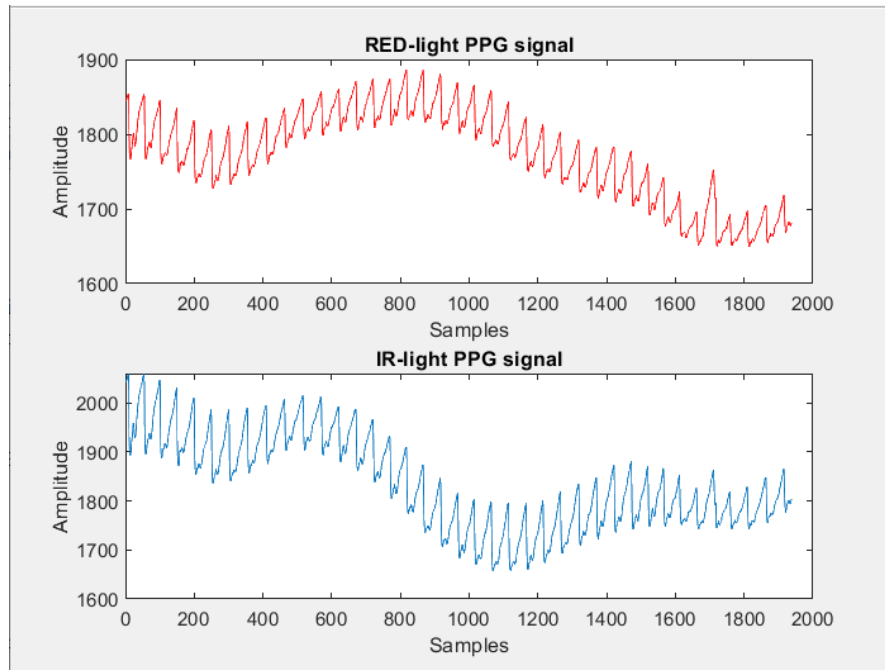


**Figure 4.8:** PPG raw signals.

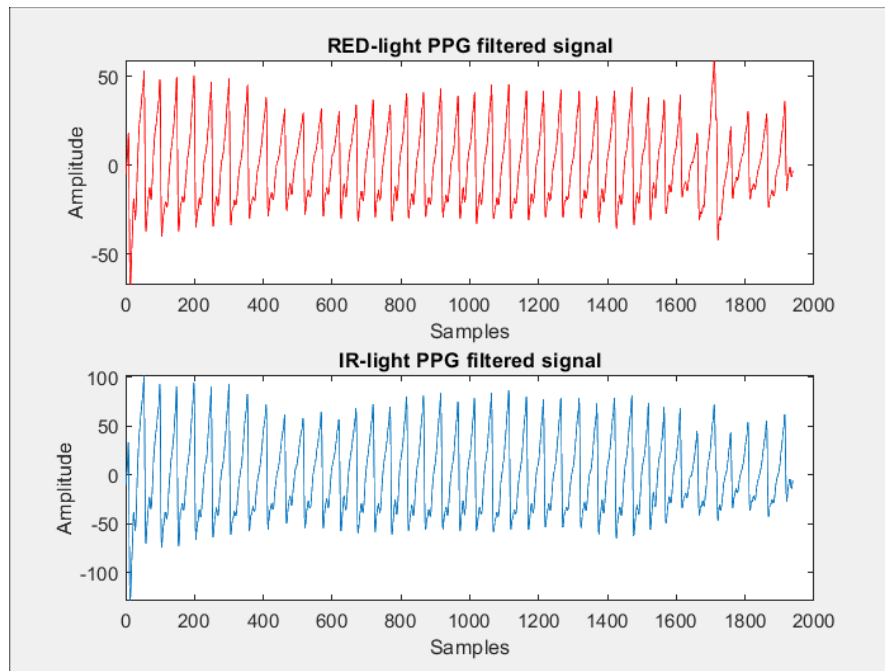


**Figure 4.9:** PPG filtered signals.

#### 4.2.1 Algorithm for calculating PR

As described in section 2.3.2, the PPG signal is characterized by two peaks, one corresponding to the systolic phase and another to the diastolic phase. The figure below highlights the difference between the *Peak to Peak interval* and the *Pulse interval*.

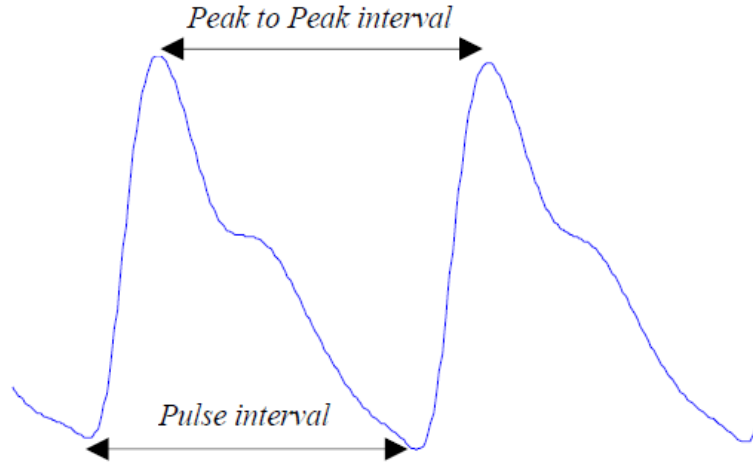


**Figure 4.10:** PPG intervals. (Source: [11])

The R-R interval in the ECG signal correlates closely with the *Peak to Peak interval* in PPG signal as both represent a completed heart cycle [11]. The *Pulse interval* is the distance between the beginning and the end of the PPG waveform. Since diastolic peaks are easier to identify than systolic peaks, in this case, the *Pulse interval* is used to calculate the PR.

The pulse frequency is calculated on a single PPG signal. This parameter can be calculated either with the signal extracted from red light with a wavelength of 660 nm or from infrared light with a wavelength of 940 nm. From what emerged in the study, the signal extracted by IR is less disturbed and lends itself better to the calculation of this parameter.

Below is shown the flowchart of the algorithm for calculating the PR.



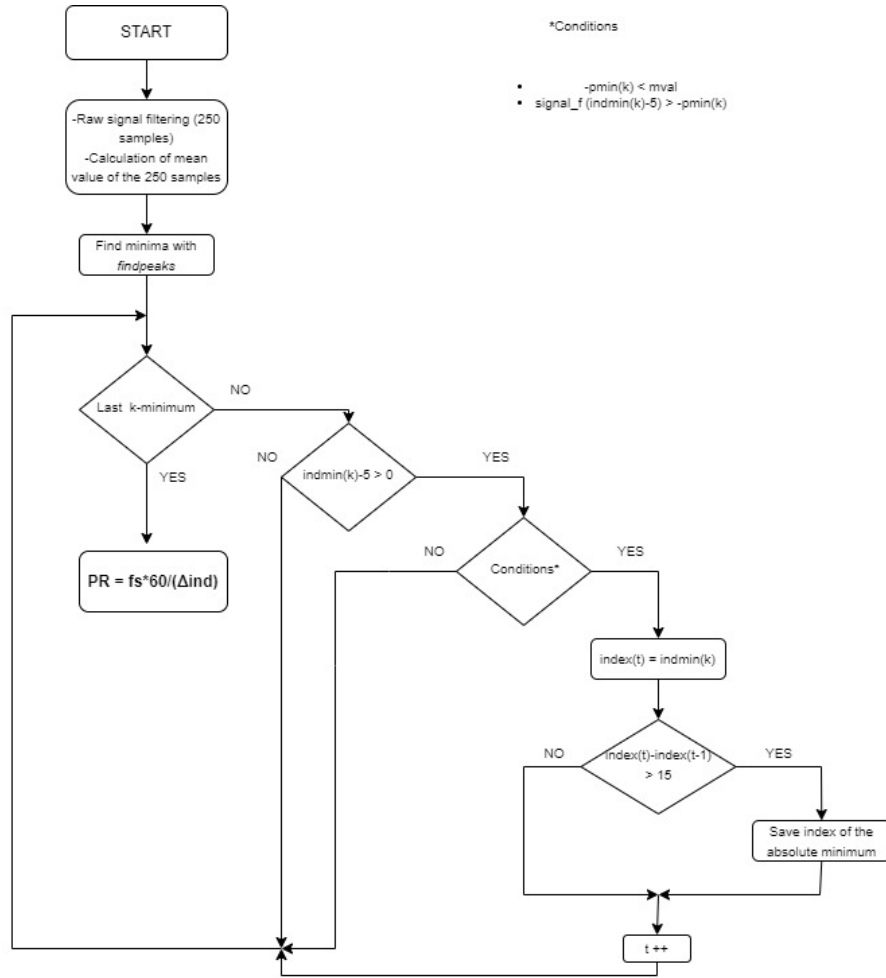


**Figure 4.11:** Flowchart of the algorithm for calculating PR.

The algorithm shown in the figure is based on identifying the minima of the window of 250 signal samples taken into account each time. The *findpeaks()* function returns the index and value of all the minima in the window considered. Through a for-loop repeated k-times, where k represents the number of minima found, the absolute minima are identified and selected. The conditions for distinguishing absolute minima from relative minima are summarised in the figure 4.11 and the code in Appendix B. After identifying the absolute n-minima, the n-1 values of PR obtained are averaged with each other to obtain more precise values. The fourth condition in the for-loop is that the index difference between two successive absolute minima must be greater than 15 samples. Therefore, the maximum calculable frequency is 200 bpm, while the minimum, as mentioned above, is 30 bpm. The values of PR that a healthy adult should have are between 60-100 bpm, while for

children, it varies between 70-130 bpm. For well-trained athletes, values are around 40-60 bpm.

Therefore, this device makes possible the monitoring of PR for a good portion of the population with different age groups.

### 4.2.2 Algorithms for calculating $\text{SpO}_2$

As mentioned in the section 2.3.1, for the calculation of arterial oxygen saturation, it is necessary to find the "ratio of ratios"  $R$  between the AC and DC components of the signals derived from the Red and IR LEDs.

Also for the calculation of  $R$  on which the  $\text{SpO}_2$  value is based, it is necessary to filter the signal as in the previous case for the PR.

The arithmetic mean of the 250-sample recursive windows is chosen as an approximation for the DC component of the signals. This average is performed on the unfiltered signal, as the high-pass filter removes the DC and the lower frequencies components.

Instead, the AC component of the signals represents the difference in amplitude from peak to valley. The calculation of the AC component is performed on the filtered signal, unlike the DC component, to avoid the error due to baseline wander. This method requires low noise data to identify peaks and valleys correctly. A further method that is suitable to moderate levels of noise, but susceptible to rapid DC changes, is to calculate the root mean square (RMS) deviation of the signal [23]. In this study, both algorithms, based on the informations derived from literature [22][23], are implemented and subsequently tested.

- **Algorithm 1:** Peaks and Valleys method

As in the algorithm for the calculation of PR, the function *findpeaks()* identifies all minima and maxima within the two filtered signals. As previously described, the values of the DC components are calculated on the unfiltered signals as the average of the 250 samples taken into consideration. The absolute minima and maxima are selected with the same conditions as presented in the flowchart in *fig.* 4.11. After identifying the peaks and valleys for the considered signal window, the AC component is calculated for both signals as the difference in amplitude between one peak and the consecutive valley. The  $n$ -values obtained are then averaged to obtain  $\text{AC}_R$  and  $\text{AC}_{IR}$ . Finally, the ratio  $R$  is derived according to equation 2.9. *Fig.* 4.12 depicts the flowchart of algorithm 1, while Appendix B shows its MATLAB code.

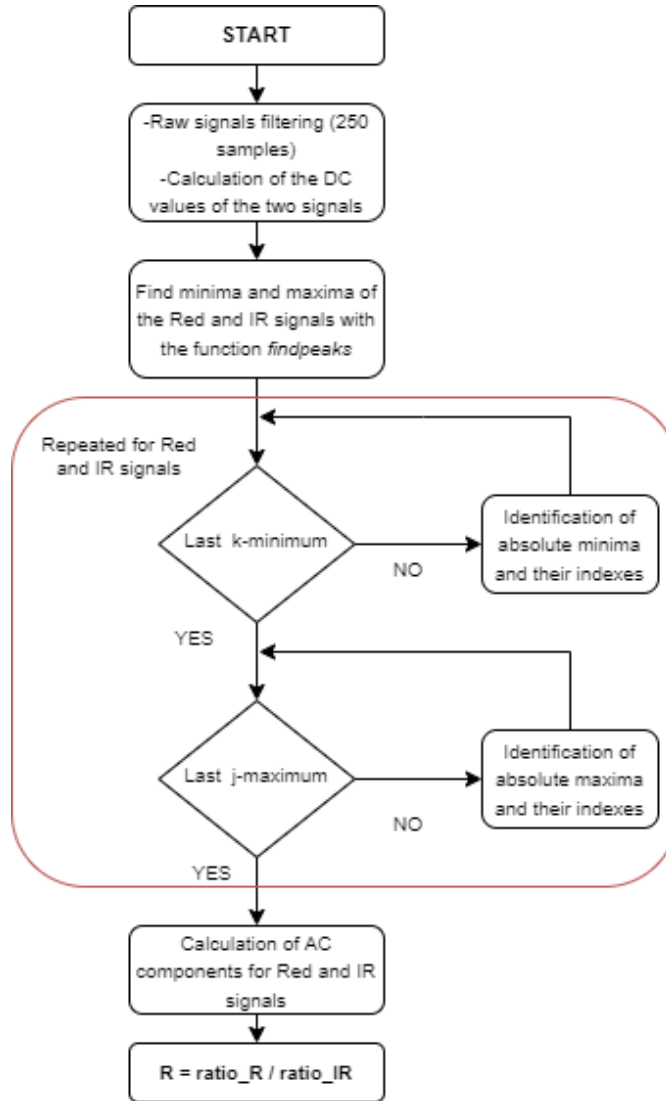


**Figure 4.12:** Flowchart of the algorithm 1 for calculating SpO<sub>2</sub>.

- **Algorithm 2:** Root-Mean-Square method

The definition of RMS is given by the following equation:

$$RMS = \sqrt{\frac{\sum_{i=1}^N x_i^2}{N}} \quad (4.1)$$

In this case, it is not essential the DC component since the RMS values are calculated only on the filtered signals. The RMS value for both signals is

obtained through the Matlab function *rms()*. Finally, the ratio *R* is calculated as the ratio of the two values  $RMS_{RED}$  and  $RMS_{IR}$ .

The MATLAB code for algorithm 2 is shown below:

```
function [RoR] = arterialoxysat_rms(signal1,signal2,c,ka,kb)

signal1_f = filtfilt(kb,ka,signal1(((c-1)*250+1): c*250+5));
signal2_f = filtfilt(kb,ka,signal2(((c-1)*250+1): c*250+5));

RMS_R = rms(signal1_f);
RMS_IR = rms(signal2_f);

RoR = RMS_R/RMS_IR;
```

### Calibration curve

After obtaining the *R* value, the next step is creating an appropriate calibration curve *R vs SpO<sub>2</sub>* to estimate the arterial oxygen saturation correctly. The calibration of the constructed device involves the use of a reference instrument: in this study, an OXY-2 pulse oximeter from GIMA is used. Its specifications are summarized in the following table.

Specification	Value
Pulse Rate Measuring Range	30bpm - 250bpm
SpO <sub>2</sub> Measuring Range	0%-100%
Measurment Accuracy for PR	±2bpm
Measurment Accuracy for SpO <sub>2</sub>	±2% in the stage 70%-100%

**Table 4.1:** GIMA OXY-2 specifications.

The *R* values calculated through the algorithm and the relative SpO<sub>2</sub> values read on the reference device are reported in a look-up table. All the values taken into account are measured on the same subject with several measurements during different days. According to this table, the calibration line is obtained.

For what concerns Algorithm 1, the calibration line is reported in *fig. 4.13*. The equation of the fitting line is:

$$SpO_2 = 110.81 - 21.908 \cdot R \quad (4.2)$$

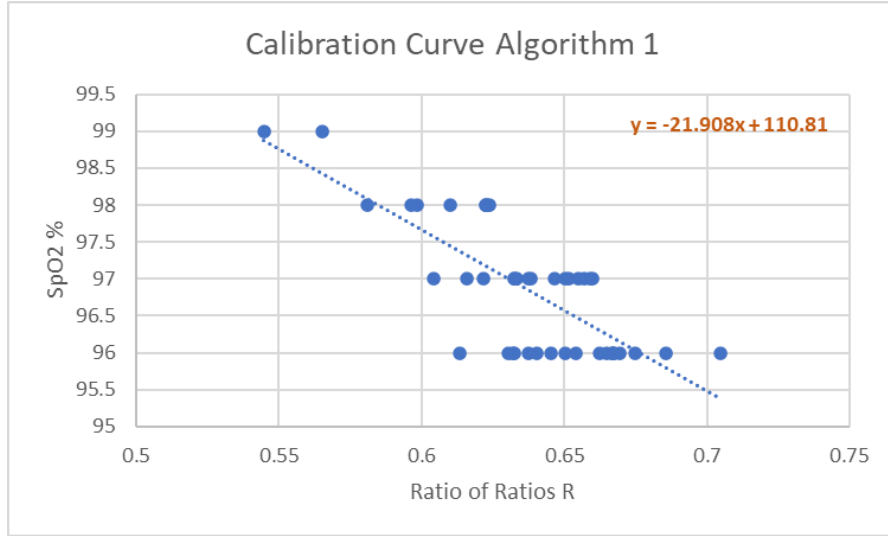


**Figure 4.13:** Calibration line for Algorithm 1.

The same procedure is repeated for Algorithm 2. *Fig. 4.14* shows the calibration line for Algorithm 2, which equation is:

$$SpO_2 = 111.26 - 22.798 \cdot R \quad (4.3)$$

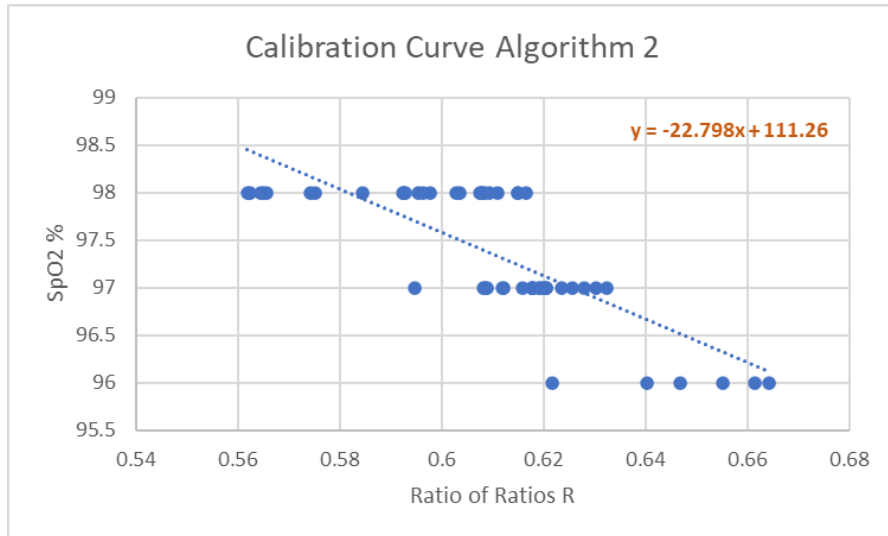


**Figure 4.14:** Calibration line for Algorithm 2.

An important parameter for comparing the two calibration straight lines is the coefficient of determination  $R^2$ , which indicates the goodness of fit for a linear

regression model. The parameters for the two lines are similar and are around 0.6, although the coefficient for algorithm 2 is higher and thus indicates a line that better represents the data. In addition to this consideration, it is essential to emphasize that algorithm 1 is more suitable for signals with low noise. Finally, experimental tests on the same subject show that algorithm 2 is more accurate in its measurements for calculating  $\text{SpO}_2$ , albeit by a small margin. Therefore algorithm 2 is selected for the experimental tests on different subjects.

### 4.2.3 Algorithm for calculating PRV

PRV is the variability of IBIs derived from a pulse wave signal. As expressed in the section 2.3.2, there is a fundamental difference between HRV and PRV. Particularly, HRV is obtained from the timings of electrical impulses causing ventricular contraction, whereas PRV is obtained from the timings of pulse waves arriving at the periphery [22]. The time difference between the electrical impulses and pulse wave arrival consists of the pre-ejection period and the pulse transit time (PPT). The pre-ejection period is the time between the impulses and ejection of blood into the aorta, while the PTT is the time taken for the pulse wave to propagate from the heart to the measurement site [22].

The algorithm for calculating the PRV is based on identifying the absolute minima of the IR signal alone, again chosen because it is less noisy and has a greater amplitude than the red signal. After determining all the minima, using the same method as in the flowchart in *fig. 4.11*, the difference in time (ms) between the successive IBIs is calculated. The n-values of PRV calculated on a window of 250 filtered signal samples are averaged again to obtain more accurate values. The flowchart of the code for calculating the PRV is represented in the following image.

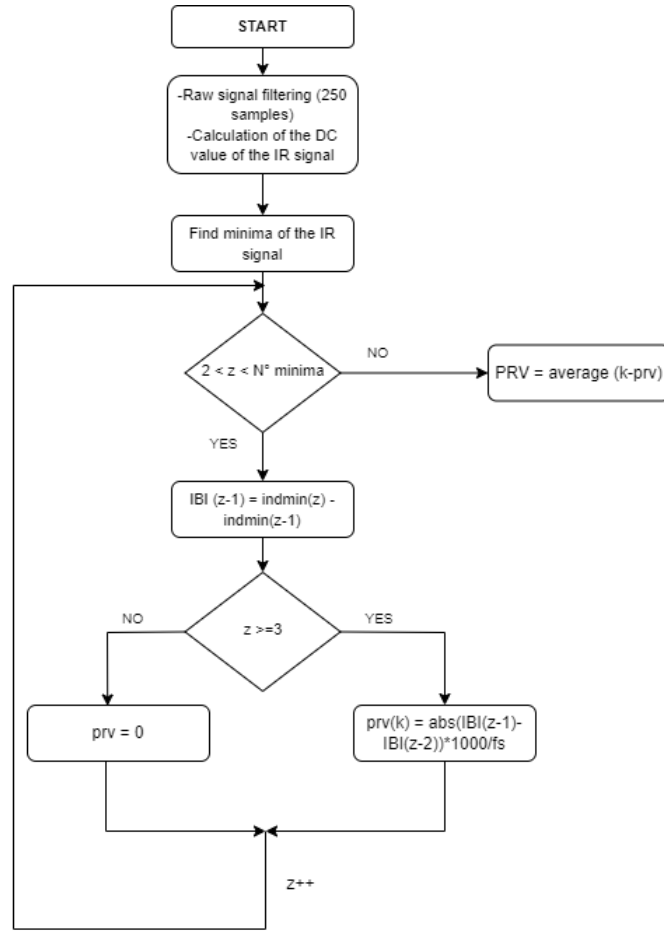


**Figure 4.15:** Flowchart of the algorithm for calculating PRV.

Younger people usually have higher HRV than older people, and males may have slightly higher HRV than females [24]. Additionally, elite athletes tend to have greater HRV than non-athletes. For example, the middle half of 25-year-old males fall roughly from 50-100 (ms), while 45-year-olds are around 35-60 (ms). Females of the same ages see a similar dip, from about 45-90 to 30-55 (ms) [24]. However, what represents a healthy HRV varies for everybody [24].

## Chapter 5

# Verification of the device and GUI design

The GIMA OXY-2 pulse oximeter is used as reference instrument to verify and validate the developed device's operation. The tests are conducted on a single subject and repeated several times under different ambient light conditions. The parameters that can be compared using the GIMA pulse-oximeter are PR and SpO<sub>2</sub>. Such a device gives indications regarding the number of pulses and the SpO<sub>2</sub> value, and it has a low voltage indicator and a bar graph display.

Using the MATLAB tool *App designer*, a GUI is developed to display the signal and the information about the subject under analysis. This GUI is created as a MATLAB App that can be shared with other MATLAB users. Subsequently, this is compacted into a web app that can also be shared via URL with non-MATLAB users.

### 5.1 Verification and validation of device operation

As described, PR and SpO<sub>2</sub> data obtained from a 60-second signal are saved in MATLAB arrays to verify the operation of the device created. Instead, the data read by the GIMA pulse oximeter are collected in a table and used to compare the device's functioning. For what concerns SpO<sub>2</sub> calculation, it is important to underline that Algorithm 2, presented in subsection 4.2.2, is used.

The test is performed on a subject at rest, sitting with the arms positioned on a table at approximately heart height. The measurements are taken in a room illuminated by ambient light, not artificial light. Data acquisition is carried out on the same subject simultaneously with the two devices. Specifically, the developed



device acquires the signal from the right index finger and the GIMA pulse oximeter from the right middle finger. Previous studies found that the subjects' right middle fingers measured the highest SpO<sub>2</sub> value [25]. However, this variance was very slight compared to the other fingers' readings. For this reason, a good practice is to reduce the margin for error by using a more uniform digit like the index or middle finger [25].

Table 5.1 shows the report of a comparison between the developed device and the GIMA OXY-2 over the acquisition of approximately 60 seconds to verify the device's operation and to calculate the margin of error with the reference device.

PR device [bpm]	PR GIMA [bpm]	SpO <sub>2</sub> device [%]	SpO <sub>2</sub> GIMA [%]
75	73	97	96
83	81	98	96
81	82	98	97
81	82	98	98
79	80	98	96
83	78	98	98
77	79	97	98
83	78	97	97
84	80	97	97
82	79	97	96
81	79	97	97
81	79	97	97
86	83	97	97
86	82	97	97

**Table 5.1:** Comparison PR and SpO<sub>2</sub> values between the developed device and GIMA OXY-2 on 60-second of signal.

The graphs with the trends of the parameters calculated for each of the two devices better visualize the comparison between the measurements.

As can be seen from Figures 5.1-5.2, there are variations in the readings of the two devices for both parameters. There is a difference in the test between the two devices concerning the PR. When analyzing the data, the developed device has higher readings for PR than GIMA. In the considered test, the values of PR read by the manufactured device differ from the reference one of -2bpm/+5bpm. Averaging the fourteen values obtained during the 60 seconds, the mean PR for the first device is about 81.5 bpm, while for the GIMA is 79.7 bpm.

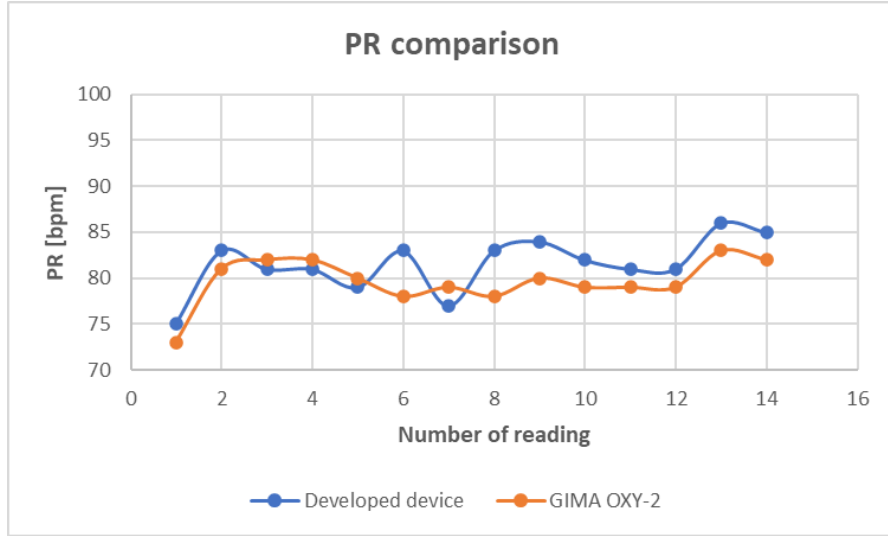


**Figure 5.1:** Comparison of PR measurments.

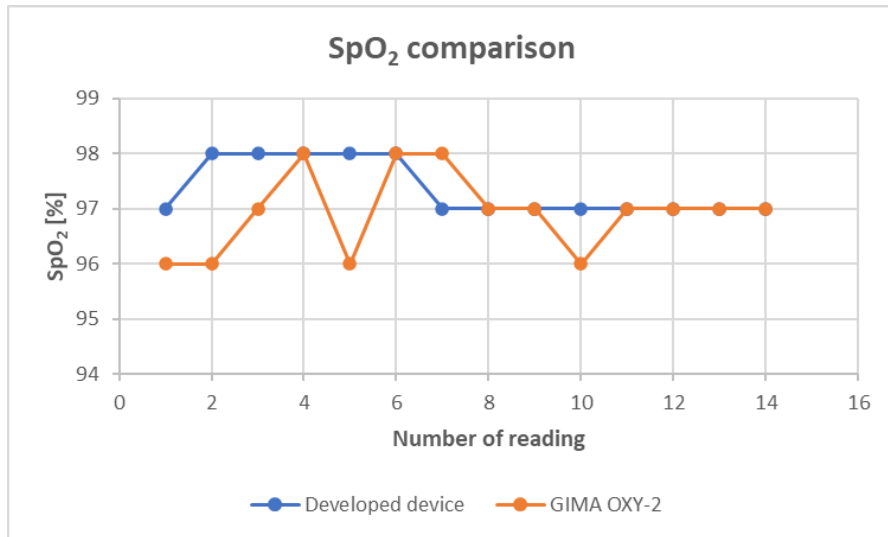


**Figure 5.2:** Comparison of SpO<sub>2</sub> measurments.

On the other hand, the measurement error between the developed device and GIMA is between  $\pm 2\%$  of the calculated arterial oxygen saturation. Regarding the the mean values, the average SpO<sub>2</sub> of the first device is 97.4%, while for the second device is 96.9%. The difference between the mean values of PR and SpO<sub>2</sub> between the two devices is minimal so that the developed device can be considered valid for use.

Factors that can affect pulse oximeter readings, in addition to rapid body

movements during readings, include external lighting and poor blood circulation [25]. Moreover, it is advisable to wash the hands before taking measurements, as a layer of dirt or dust can hinder the light's ability to reflect [25].

## 5.2 Matlab GUI design

The creation of a graphical user interface is linked to the need to monitor the progress of vital parameters in real-time and to be able to choose when to start or stop the signal acquisition. The GUI is subsequently used to develop a Matlab Web App.

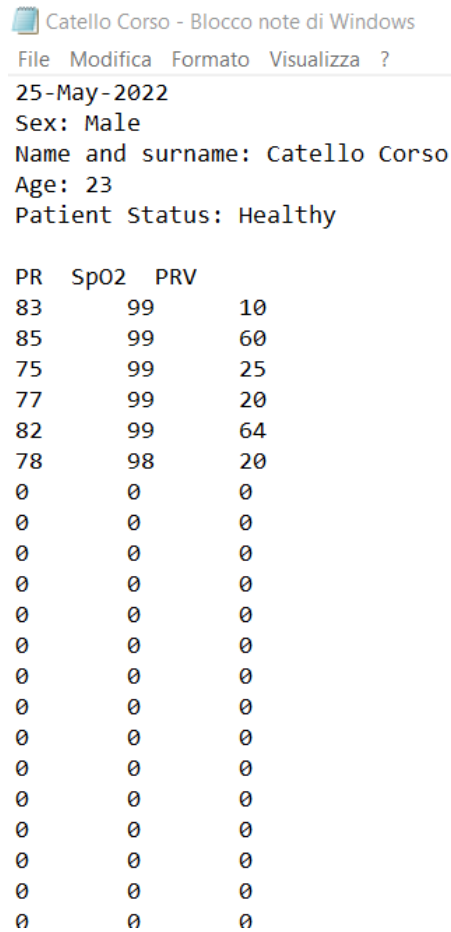
The graphical interface is created using Matlab's *App Designer* tool and allows interaction with the Arduino Due board via communication with the COM4 serial port. The purpose of the GUI is to be used by healthcare staff to monitor the patients and save all their data.

The interface created presents the possibility of filling in important informations related to the patient's identity and clinical status. Using a data picker makes it possible to select the date on which the patient's data is collected. Furthermore, by employing edit fields, it is possible to express the patient's first name, surname, age, clinical status, and gender through a button. The GUI also features axes for displaying the red and infrared signals in real-time and a table where all measured parameters are read and saved.

Three status buttons are also present: one to start the signal acquisition, another to stop it, and another to save all the data concerning the patient in a *text* file.

*Figure 5.3* represents the graphical user interface in which all the features described above are depicted. The axes show the two PPG signals acquired in real-time, while the table displays the three vital parameters. The editable fields represent the patient's information. The case presented in *fig. 5.3* shows an example of how the GUI works.





Catello Corso - Blocco note di Windows

File Modifica Formato Visualizza ?

25-May-2022  
 Sex: Male  
 Name and surname: Catello Corso  
 Age: 23  
 Patient Status: Healthy

PR	SpO2	PRV
83	99	10
85	99	60
75	99	25
77	99	20
82	99	64
78	98	20
0	0	0
0	0	0
0	0	0
0	0	0
0	0	0
0	0	0
0	0	0
0	0	0
0	0	0
0	0	0
0	0	0
0	0	0
0	0	0
0	0	0
0	0	0
0	0	0
0	0	0
0	0	0
0	0	0

**Figure 5.4:** Representation of the text file with patient's informations.

The idea of saving calculated data is to create a database for all patients followed by a particular doctor or within a medical structure, where it is necessary to monitor the patients continuously.

The graphical user interface is used to develop a MATLAB Web App that can be shared with other users via URL.

### 5.3 Development of Matlab Web App

After creating the GUI, to create a deployed web app is necessary to install the MATLAB Compiler. Through this toolbox, the *Pulse\_oximeterAPP.mlapp* file is compacted into a Content Transformation File (.ctf). The software architecture describing the telemonitoring system is depicted in *fig. 5.5*

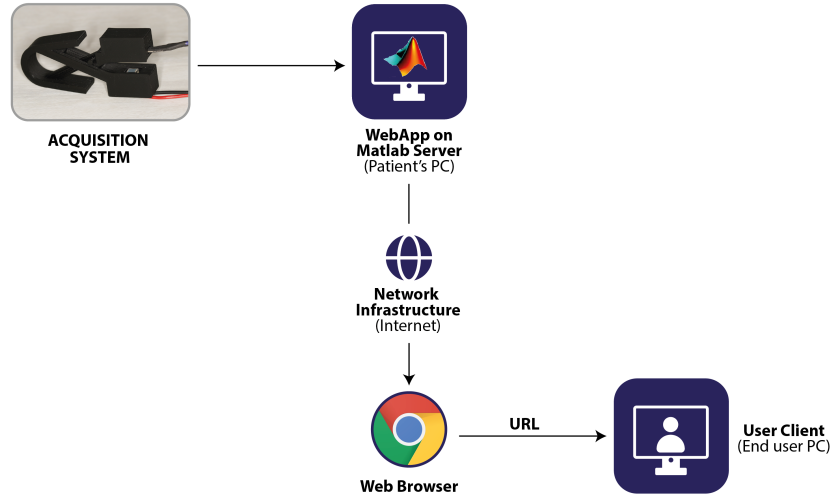


**Figure 5.5:** Software block diagram

A dedicated standalone server is used to share the app via URL with other users. In this case, the MATLAB WebAppServer is installed and set up. The MATLAB WebAppServer uses a TCP port for data transfer and sharing via URL. The 9988 port is selected by default. Usually, this port does not allow incoming connections as the system's firewall blocks them. Therefore, it is necessary to allow incoming access and modify firewall settings for port 9988. The compacted file *Pulse\_oximeterAPP2.ctf* is then added to the App Folder of the MATLAB Web App Server.

*Figure 5.6* depicts the configuration of the MATLAB Web App Server toolbox. The "Start" button and successively "Open Home Page" must be enabled to visualize the app correctly in the browser selected by default and generate the URL to share.

Once the MATLAB Web App Server has started, the created app is visible on the web browser page. This page will also show other apps, eventually made by the same user. As shown in *fig. 5.7*, the app is correctly visualized, and on the top search bar is also defined the URL linked to it. The URL is of the type: **http://ip\_address:Port/webapps/home/index.html**. For this reason,

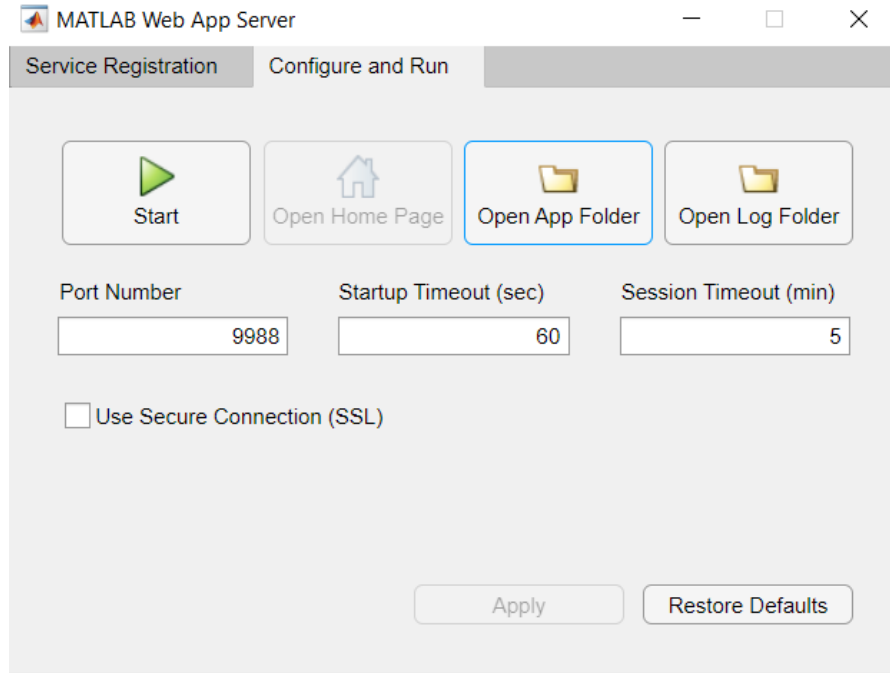


**Figure 5.6:** MATLAB Web App Server configuration.

every time the primary user is connected to a different network, the URL changes according to the private (or local) IP address of the device.

A private IP is an address the network router assigns to a specific device. Each device within the same network is set to a unique local IP address. Local IP addresses let devices connected to the same network communicate with one another without connecting to the entire internet [26]. Private IPs help bolster security within a specific network [26]. In the presented case, the URL that is useful to share the app between users connected to the same network is **http://192.168.1.149:9988/webapps/home/index.html**.

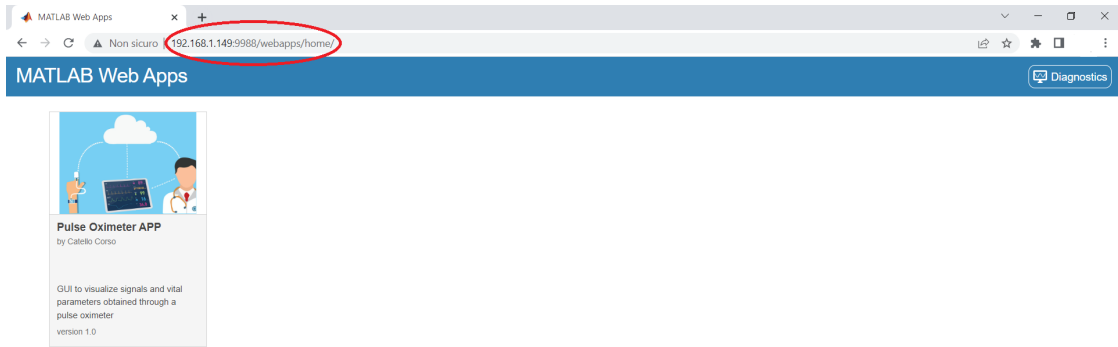


**Figure 5.7:** Visualization of the web app on *Google Chrome* browser.

On the other hand, a public IP is an address that can be accessed directly over the internet and is assigned to the network router by an internet service provider (ISP). A public IP address helps connect to the internet from inside the network to outside the network [26].

According to these considerations, it is possible to share the URL of the web app also with other users connected to a different network by using a public IP address. It is essential to change the router's settings and allow connections on public IP addresses. In this case, the URL to share is **http://79.153.81.4:9988/webapps/home/index.html**. Nevertheless, it must be underlined that if the local network changes, the public and the private IP addresses also change, and so do the URLs.



Figure 5.8 presents how the web app works on the web page.



**Figure 5.8:** Web app operation.

The end-user can also manage the same functionalities presented in the GUI. This ties with a different doctor-patient approach and the idea of possible telemonitoring of the patient by the healthcare provider.

The final chapter will present improvement options for developing the web app and making it more efficient.

## Chapter 6

# Experimental tests and results

Experimental tests are carried out to verify the functioning of the developed device on several subjects of different ages and gender. Twelve subjects aged between 23 and 73 years are considered for experimental testing of the device. Eight of them are male, and four are female. Fifty percent of the subjects analyzed are between 23 and 37 years old, and the remainder is between 56 and 73 years old. For all cases subsequently presented, the values acquired with the designed device are always compared with the GIMA OXY-2. As described in section 5.1, the developed device is inserted in the right index finger while the GIMA OXY-2 is in the right middle finger. Every subject during the acquisition is at rest, sitting and with the arms placed on the table at heart height. For each subject, the trend of the parameters in 60 seconds of the signal is assessed, so fourteen values are calculated for each parameter.

The following tables and graphs show the values obtained for both the devices and the differences between the two acquisitions. The final section of the chapter discusses the results arising from the experimental tests.

## 6.1 Experimental tests on different subjects

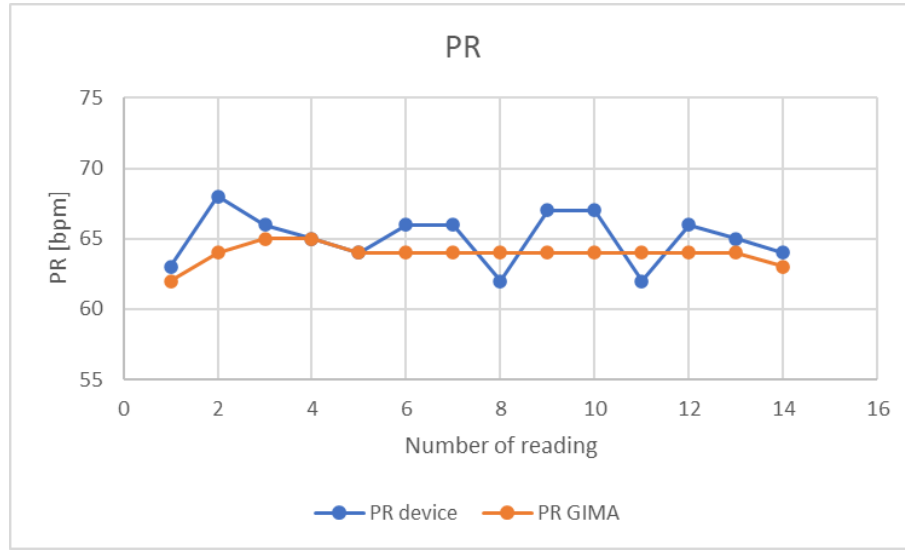
### Subject 1

- Gender: Female
- Age: 37y
- Patient Status: Healthy

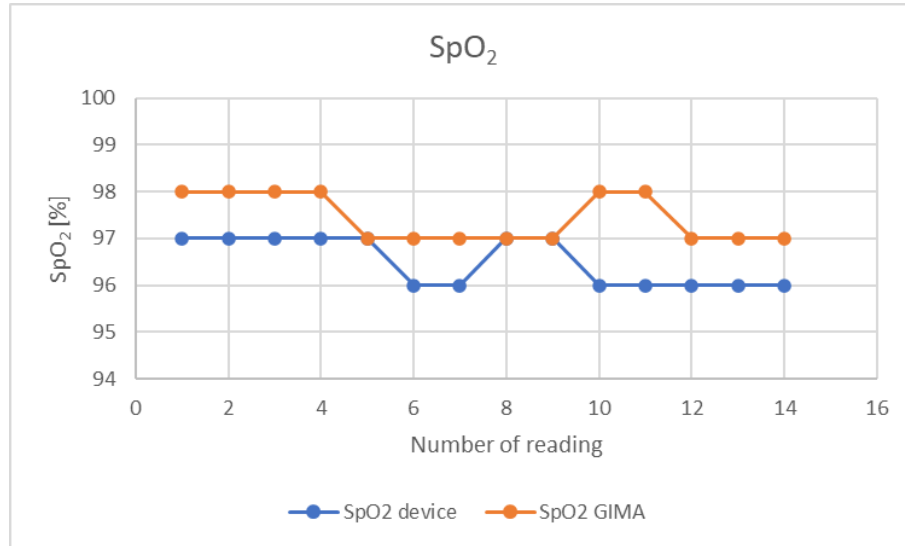
Designed device		
PR [bpm]	SpO <sub>2</sub> [%]	PRV [ms]
63	97	60
68	97	90
66	97	93
65	97	40
64	97	20
66	96	33
66	96	45
62	97	33
67	97	20
67	96	73
62	96	27
66	96	30
65	96	40
64	96	60

GIMA OXY-2	
PR [bpm]	SpO <sub>2</sub> [%]
62	98
64	98
65	98
65	98
64	97
64	97
64	97
64	97
64	97
64	98
64	98
64	97
64	97
63	97

**Table 6.1:** Subject 1 data\*.



((a)) PR comparison.



((b)) SpO<sub>2</sub> comparison.

**Figure 6.1:** Subject 1 parameters' comparison.

\*Some values are discarded because of false readings from the designed device.

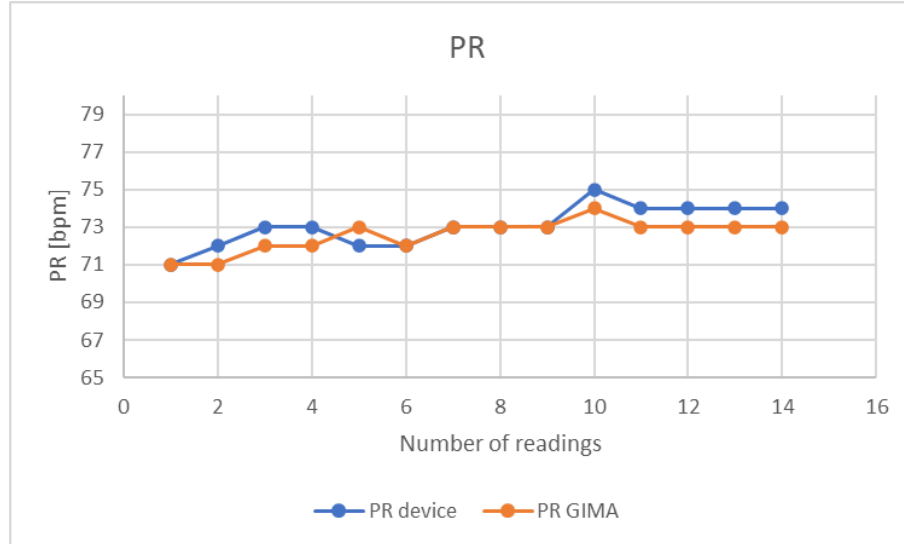
## Subject 2

- Gender: Male
- Age: 64y
- Patient Status: Healthy

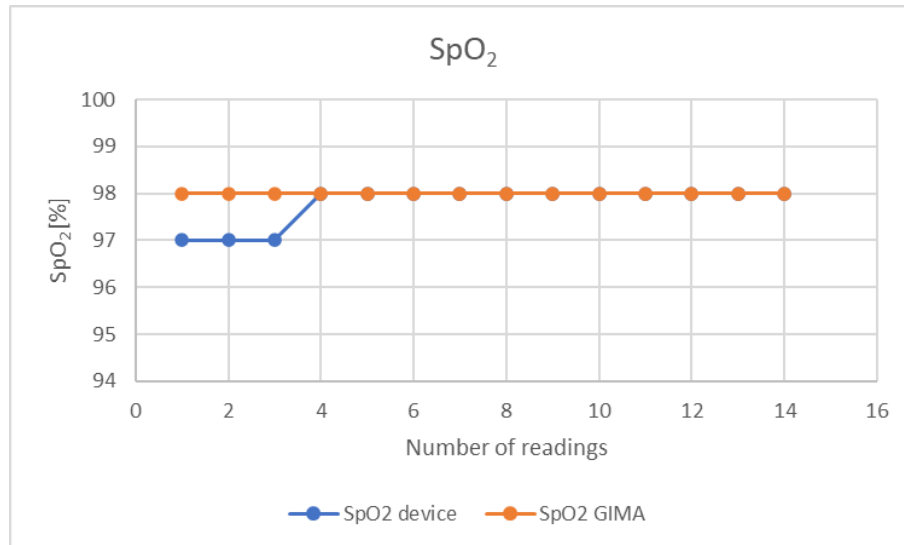
Designed device		
PR [bpm]	SpO <sub>2</sub> [%]	PRV [ms]
71	97	10
72	97	10
73	97	5
73	98	5
72	98	10
72	98	33
73	98	20
73	98	15
73	98	30
75	98	20
74	98	15
74	98	15
74	98	10
74	98	5

GIMA OXY-2	
PR [bpm]	SpO <sub>2</sub> [%]
71	98
71	98
72	98
72	98
73	98
72	98
73	98
73	98
73	98
73	98
74	98
73	98
73	98
73	98
73	98

**Table 6.2:** Subject 2 data.



((a)) PR comparison.



((b)) SpO<sub>2</sub> comparison.

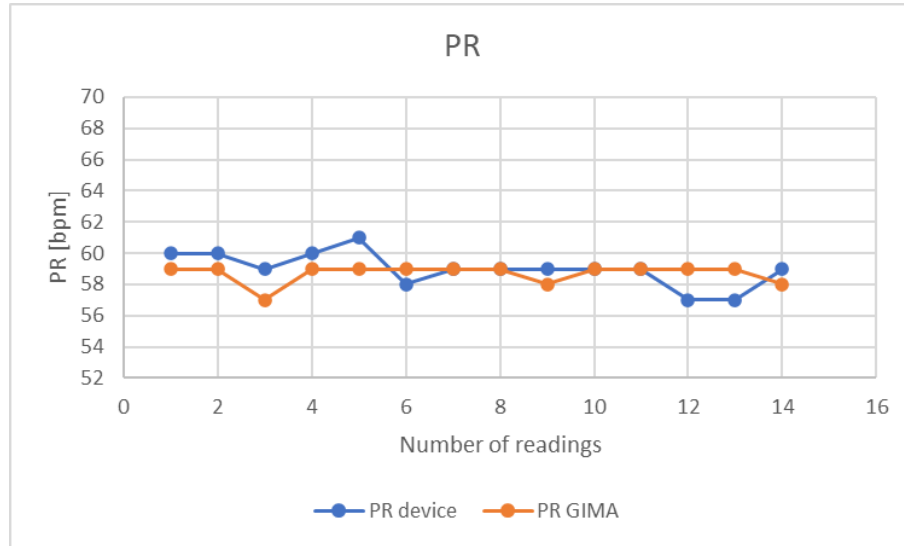
**Figure 6.2:** Subject 2 parameters' comparison.

### Subject 3

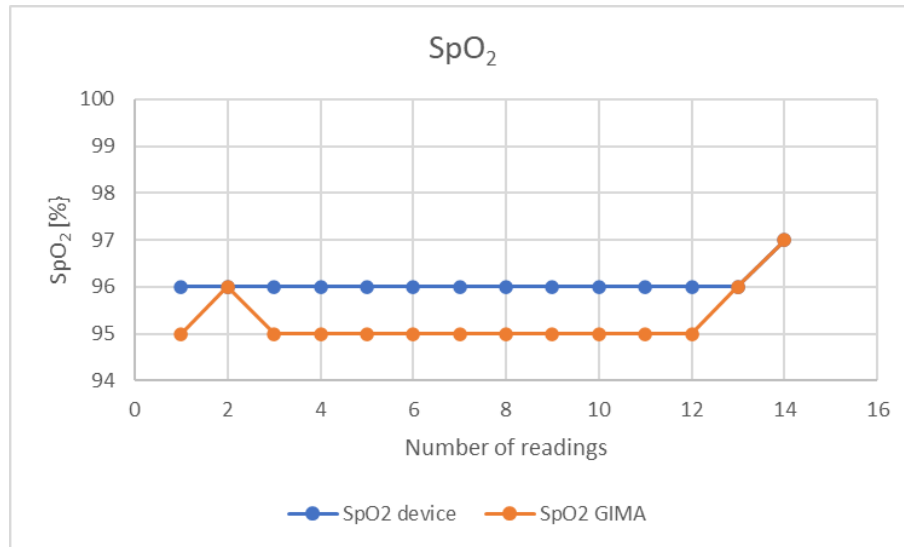
- Gender: Female
- Age: 62y
- Patient Status: Healthy

Designed device			GIMA OXY-2	
PR [bpm]	SpO <sub>2</sub> [%]	PRV [ms]	PR [bpm]	SpO <sub>2</sub> [%]
60	96	20	59	95
60	96	20	59	96
59	96	33	57	95
60	96	40	59	95
61	96	40	59	95
58	96	40	59	95
59	96	20	59	95
59	96	30	59	95
59	96	27	58	95
59	96	27	59	95
59	96	7	59	95
57	96	20	59	95
57	96	13	59	96
59	97	20	58	97

**Table 6.3:** Subject 3 data.



((a)) PR comparison.



((b)) SpO<sub>2</sub> comparison.

**Figure 6.3:** Subject 3 parameters' comparison.



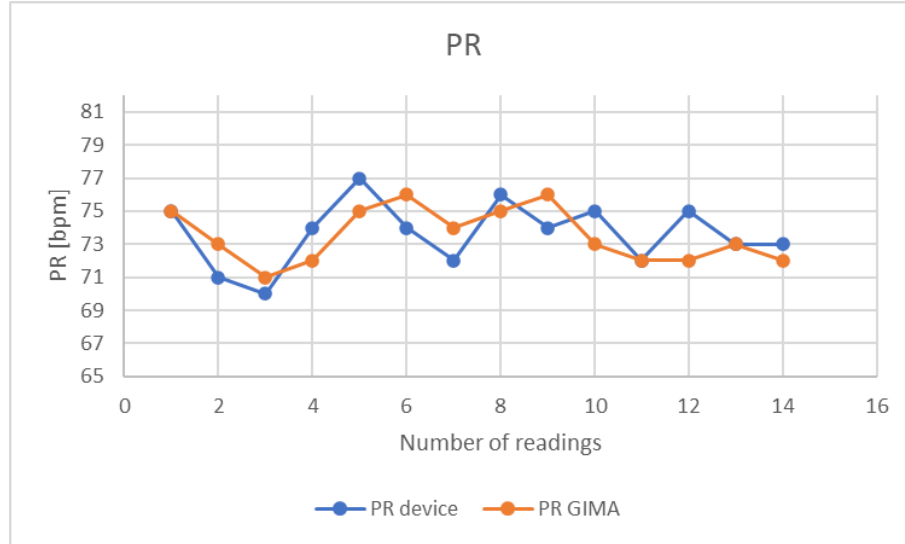
#### Subject 4

- Gender: Female
- Age: 73y
- Patient Status: Healthy

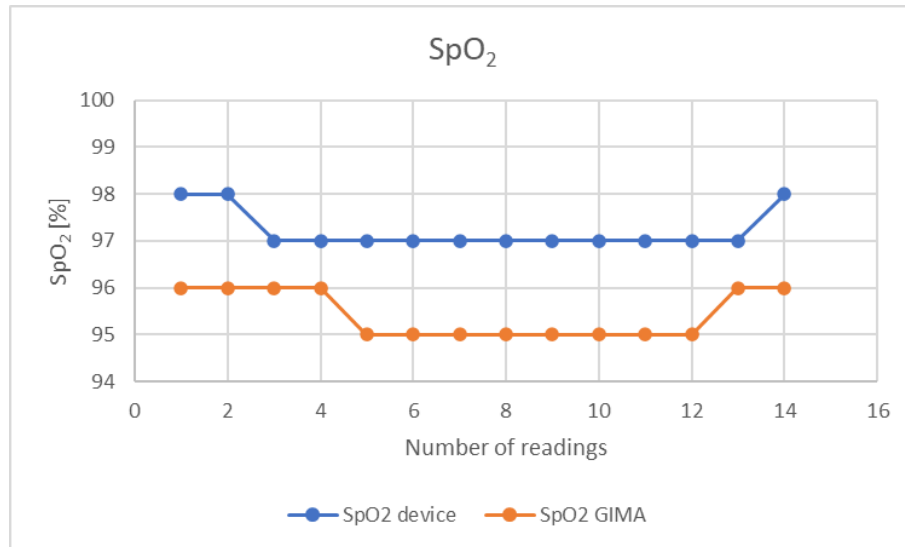
Designed device		
PR [bpm]	SpO <sub>2</sub> [%]	PRV [ms]
75	98	35
71	98	40
70	97	10
74	97	15
77	97	24
74	97	30
72	97	15
76	97	10
74	97	35
75	97	25
72	97	13
75	97	28
73	97	30
73	98	25

GIMA OXY-2	
PR [bpm]	SpO <sub>2</sub> [%]
75	96
73	96
71	96
72	96
75	95
76	95
74	95
75	95
76	95
73	95
72	95
72	95
73	96
72	96

**Table 6.4:** Subject 4 data.



((a)) PR comparison.



((b)) SpO<sub>2</sub> comparison.

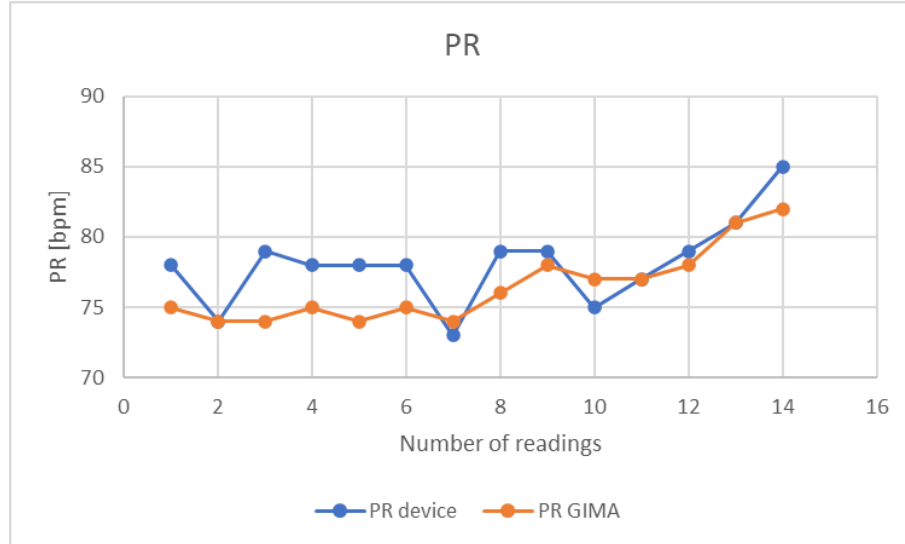
**Figure 6.4:** Subject 4 parameters' comparison.

### Subject 5

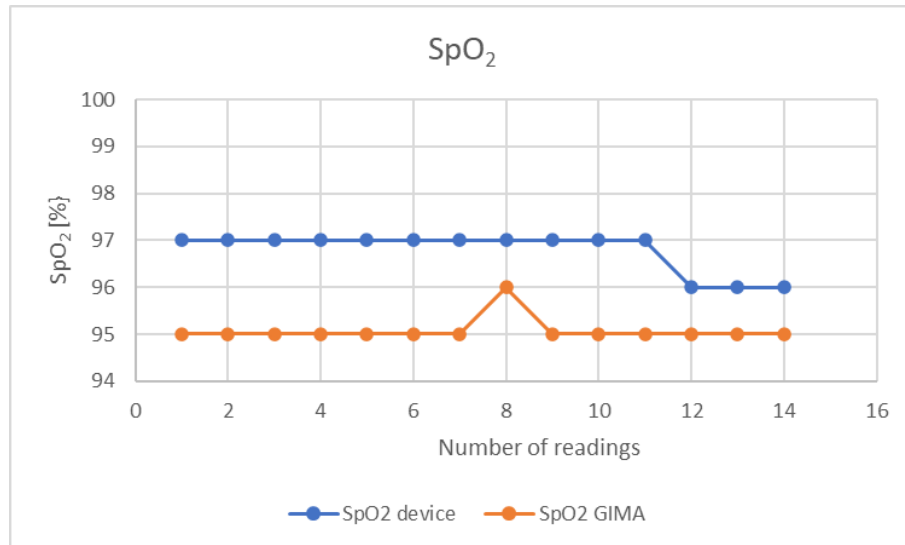
- Gender: Male
- Age: 24y
- Patient Status: Healthy

Designed device			GIMA OXY-2	
PR [bpm]	SpO <sub>2</sub> [%]	PRV [ms]	PR [bpm]	SpO <sub>2</sub> [%]
78	96	40	75	95
74	96	35	74	95
79	97	50	74	95
78	97	36	75	95
78	97	30	74	95
78	97	33	75	95
73	97	50	74	95
79	97	30	76	96
79	97	35	78	95
75	97	68	77	95
77	96	73	77	95
79	96	30	78	95
81	96	30	81	95
85	96	60	82	95

**Table 6.5:** Subject 5 data.



((a)) PR comparison.



((b)) SpO<sub>2</sub> comparison.

**Figure 6.5:** Subject 5 parameters' comparison.

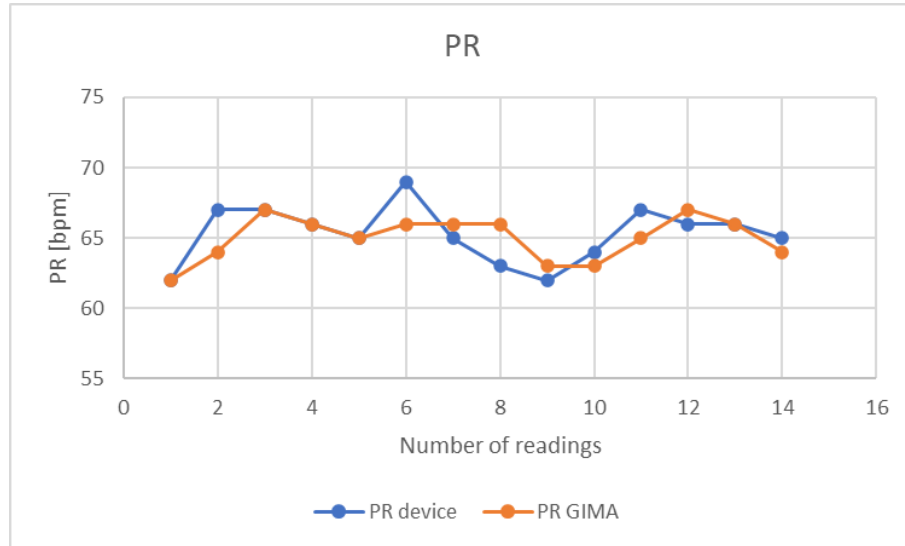
### Subject 6

- Gender: Female
- Age: 67y
- Patient Status: Healthy

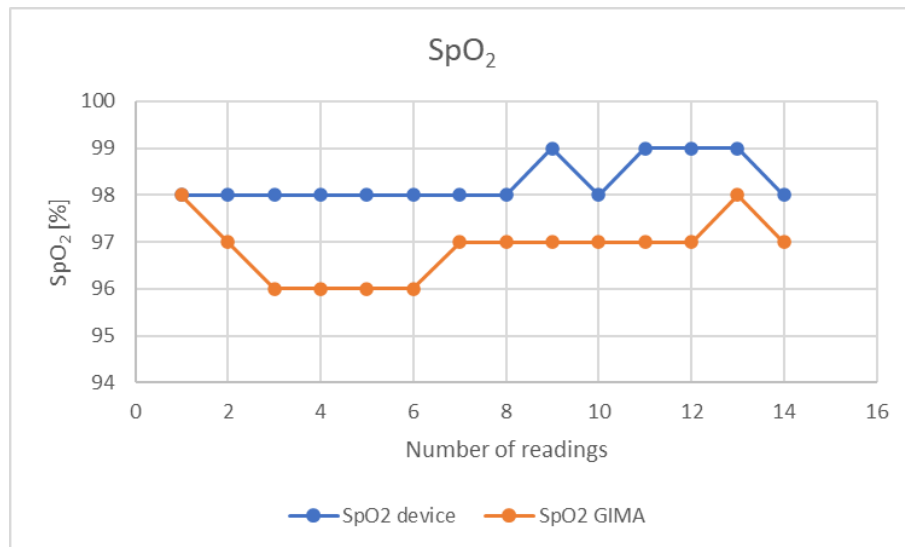
Designed device		
PR [bpm]	SpO <sub>2</sub> [%]	PRV [ms]
62	98	20
67	98	15
67	98	7
66	98	30
65	98	40
69	98	10
65	98	33
63	98	20
62	99	20
64	98	15
67	99	13
66	99	15
66	99	13
65	98	13

GIMA OXY-2	
PR [bpm]	SpO <sub>2</sub> [%]
62	98
64	97
67	96
66	96
65	96
66	96
66	97
66	97
63	97
63	97
65	97
67	97
66	98
64	97

**Table 6.6:** Subject 6 data.



((a)) PR comparison.



((b)) SpO<sub>2</sub> comparison.

**Figure 6.6:** Subject 6 parameters' comparison.

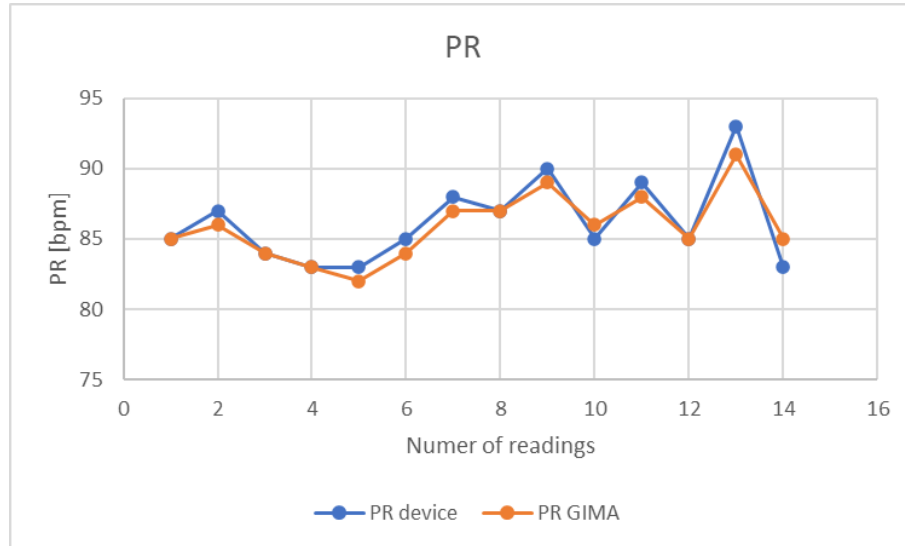
### Subject 7

- Gender: Male
- Age: 32y
- Patient Status: Smoker

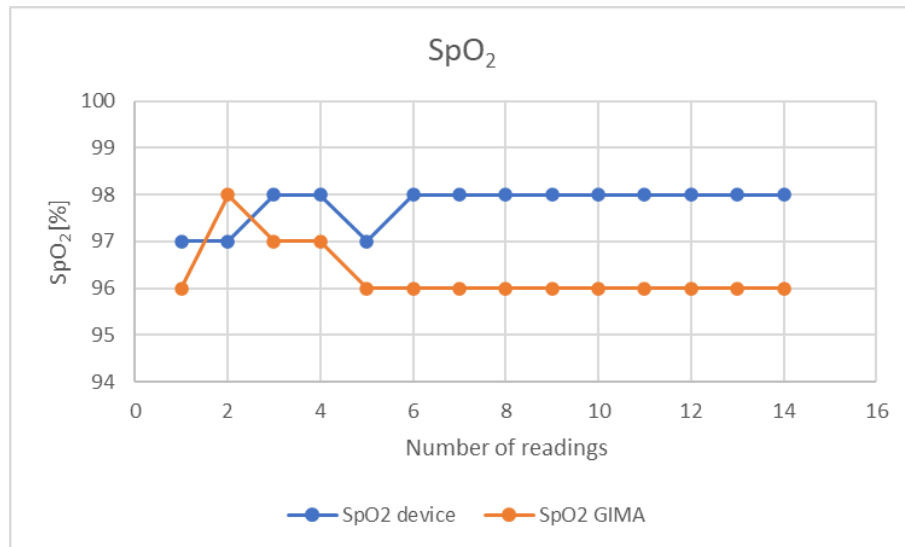
Designed device		
PR [bpm]	SpO <sub>2</sub> [%]	PRV [ms]
85	97	40
87	97	10
84	98	15
83	98	16
83	97	20
85	98	30
88	98	20
87	98	12
90	98	12
85	98	20
89	98	10
85	98	15
93	98	10
83	98	16

GIMA OXY-2	
PR [bpm]	SpO <sub>2</sub> [%]
85	96
86	98
84	97
83	97
82	96
84	96
87	96
87	96
89	96
86	96
88	96
85	96
91	96
85	96

**Table 6.7:** Subject 7 data.



((a)) PR comparison.



((b)) SpO<sub>2</sub> comparison.

**Figure 6.7:** Subject 7 parameters' comparison.



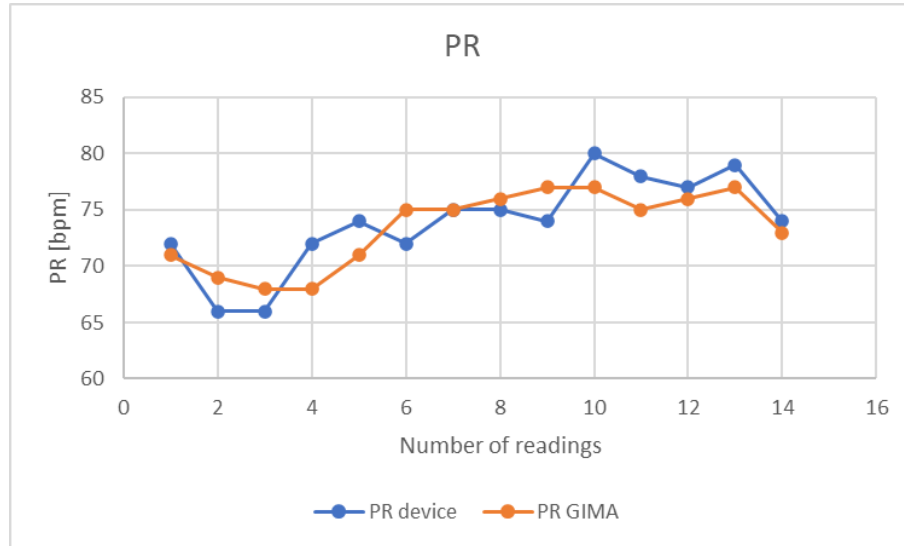
### Subject 8

- Gender: Male
- Age: 23y
- Patient Status: Healthy

Designed device		
PR [bpm]	SpO <sub>2</sub> [%]	PRV [ms]
72	99	35
66	99	20
66	99	30
72	99	15
74	99	105
72	99	20
75	99	15
75	99	30
74	99	20
80	99	68
78	98	72
77	98	70
79	98	75
74	98	50

GIMA OXY-2	
PR [bpm]	SpO <sub>2</sub> [%]
71	99
69	98
68	98
68	97
71	97
75	97
75	97
76	97
77	97
77	98
75	98
76	98
77	98
73	98

**Table 6.8:** Subject 8 data.



((a)) PR comparison.



((b)) SpO<sub>2</sub> comparison.

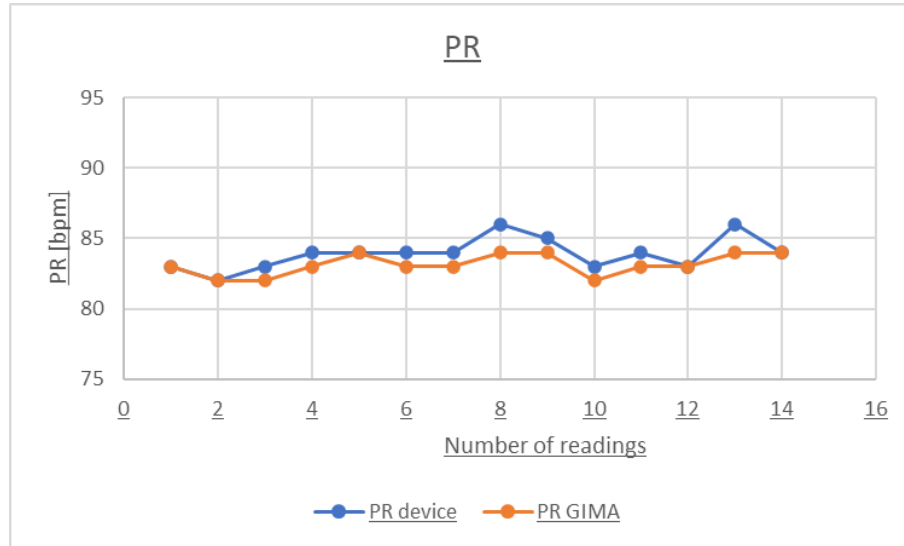
**Figure 6.8:** Subject 8 parameters' comparison.

### Subject 9

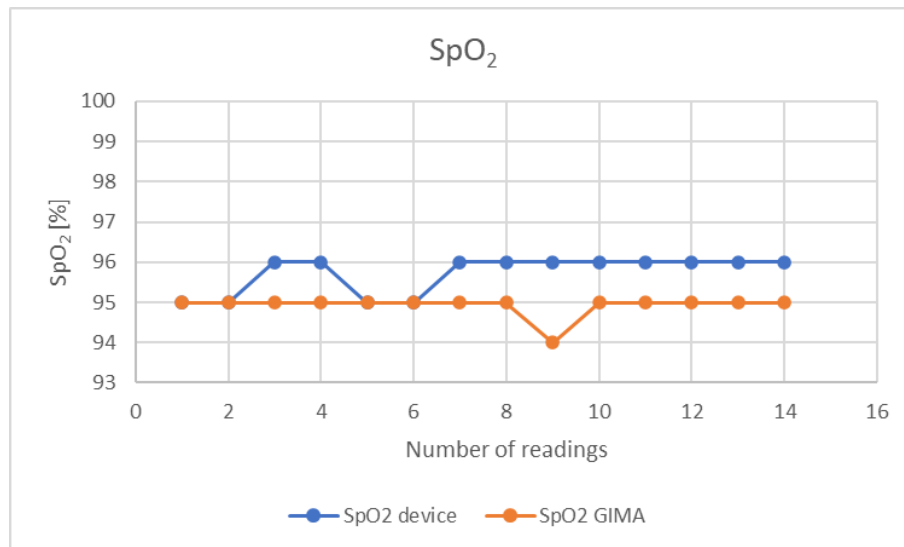
- Gender: Male
- Age: 66y
- Patient Status: Susceptible to pneumonia

Designed device			GIMA OXY-2	
PR [bpm]	SpO <sub>2</sub> [%]	PRV [ms]	PR [bpm]	SpO <sub>2</sub> [%]
83	95	12	83	95
82	95	28	82	95
83	96	10	82	95
84	96	15	83	95
84	95	20	84	95
84	95	10	83	95
84	96	10	83	95
86	96	12	84	95
85	96	32	84	94
83	96	10	82	95
84	96	15	83	95
83	96	15	83	95
86	96	10	84	95
84	96	45	84	95

**Table 6.9:** Subject 9 data.



((a)) PR comparison.



((b)) SpO<sub>2</sub> comparison.

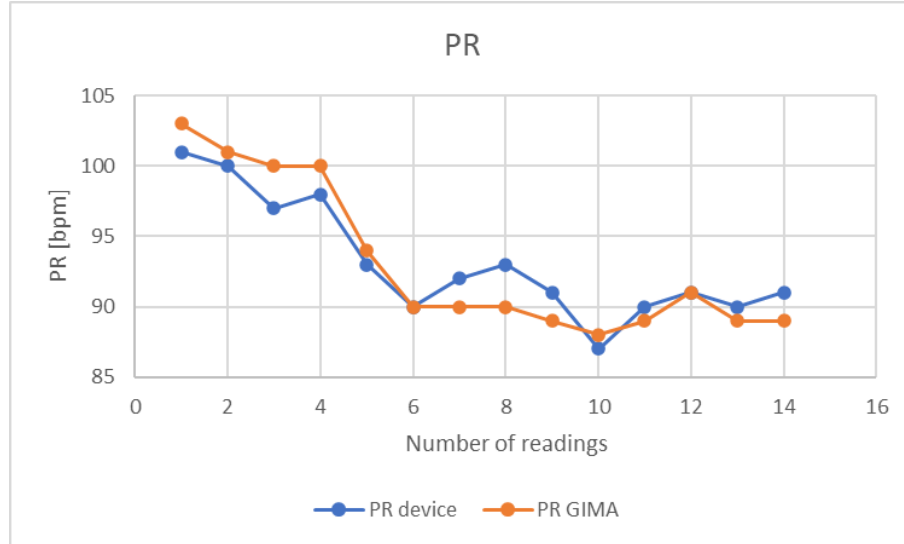
**Figure 6.9:** Subject 9 parameters' comparison.

### Subject 10

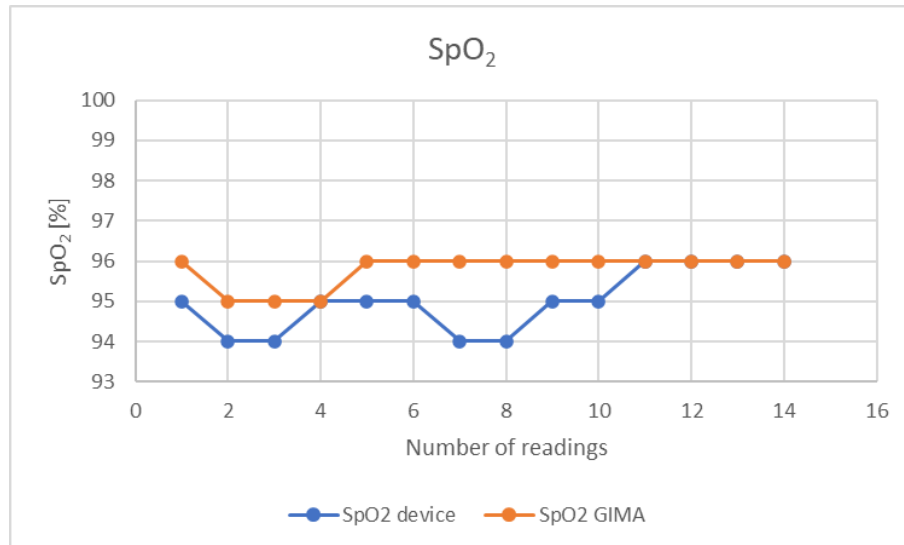
- Gender: Male
- Age: 24y
- Patient Status: Healthy

Designed device			GIMA OXY-2	
PR [bpm]	SpO <sub>2</sub> [%]	PRV [ms]	PR [bpm]	SpO <sub>2</sub> [%]
101	95	103	103	96
100	94	20	101	95
97	94	36	100	95
98	95	63	100	95
93	95	40	94	96
90	95	28	90	96
92	94	23	90	96
93	94	23	90	96
91	95	33	89	96
87	95	40	88	96
90	96	40	89	96
91	96	20	91	96
90	96	32	89	96
91	96	40	89	96

**Table 6.10:** Subject 10 data.



((a)) PR comparison.



((b)) SpO<sub>2</sub> comparison.

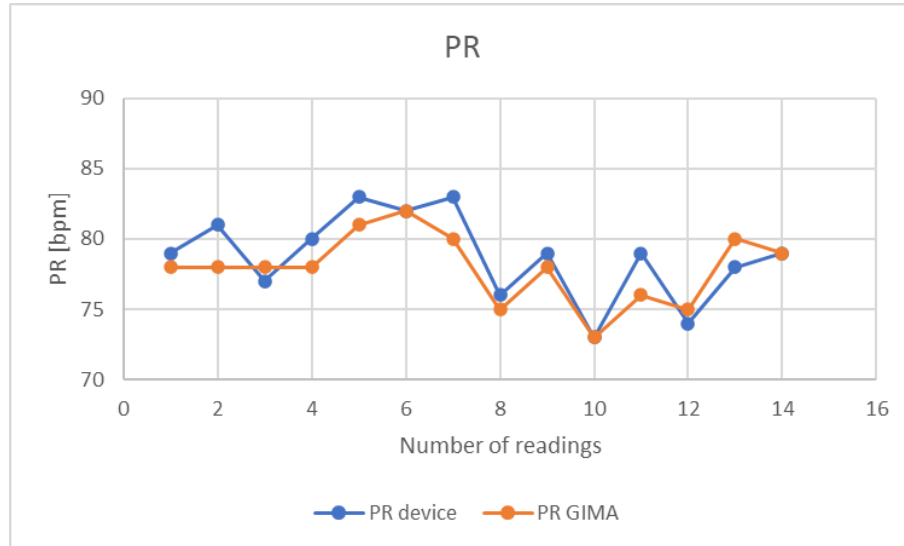
**Figure 6.10:** Subject 10 parameters' comparison.

### Subject 11

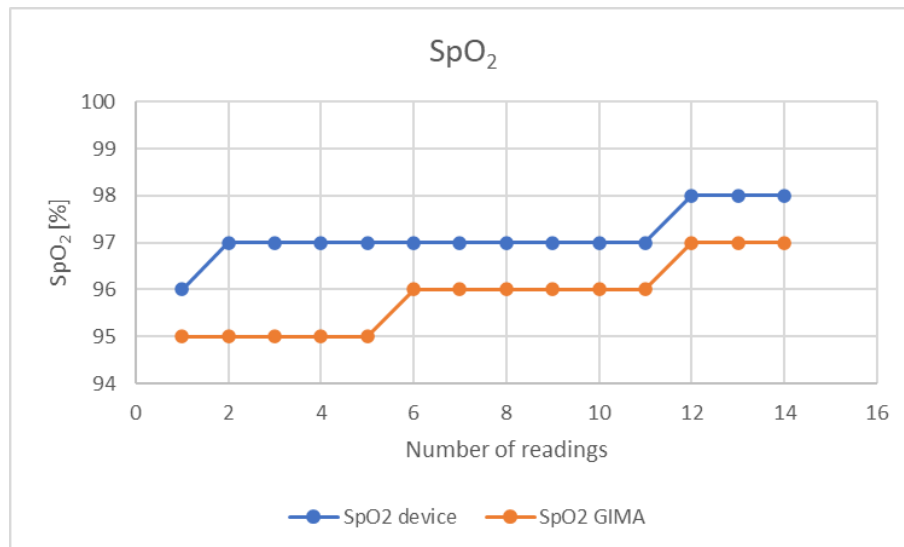
- Gender: Male
- Age: 30y
- Patient Status: Healthy

Designed device			GIMA OXY-2	
PR [bpm]	SpO <sub>2</sub> [%]	PRV [ms]	PR [bpm]	SpO <sub>2</sub> [%]
79	96	25	78	95
81	97	20	78	95
77	97	50	78	95
80	97	28	78	95
83	97	30	81	95
82	97	32	82	96
83	97	45	80	96
76	97	25	75	96
79	97	35	78	96
73	97	35	73	96
79	97	70	76	96
74	98	67	75	97
78	98	28	80	97
79	98	32	79	97

**Table 6.11:** Subject 11 data.



((a)) PR comparison.



((b)) SpO<sub>2</sub> comparison.

**Figure 6.11:** Subject 11 parameters' comparison.

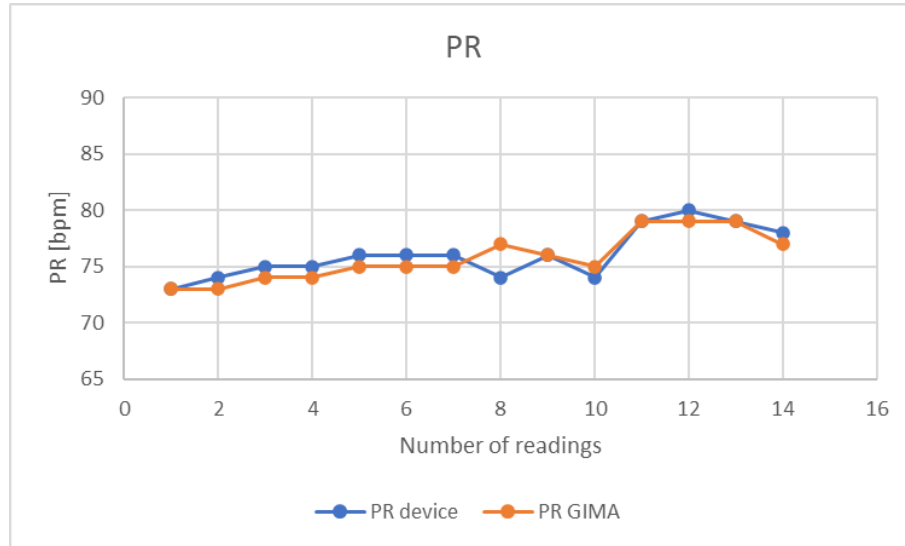


### Subject 12

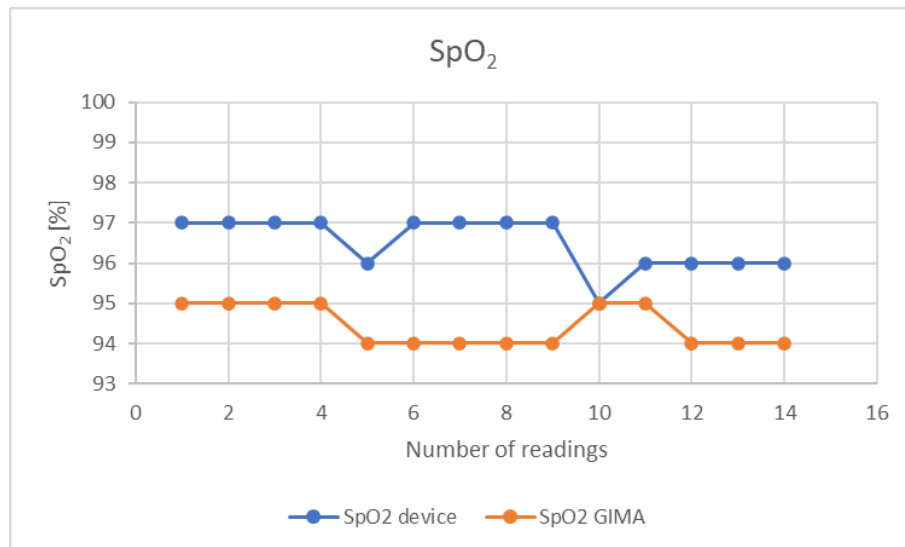
- Gender: Male
- Age: 56y
- Patient Status: Healthy

Designed device			GIMA OXY-2	
PR [bpm]	SpO <sub>2</sub> [%]	PRV [ms]	PR [bpm]	SpO <sub>2</sub> [%]
73	97	30	73	95
74	97	20	73	95
75	97	35	74	95
75	97	25	74	95
76	96	24	75	94
76	97	15	75	94
76	97	25	75	94
74	97	20	77	94
76	97	25	76	94
74	95	25	75	95
79	96	20	79	95
80	96	40	79	94
79	96	20	79	94
78	96	32	77	94

**Table 6.12:** Subject 12 data.



((a)) PR comparison.



((b)) SpO<sub>2</sub> comparison.

**Figure 6.12:** Subject 12 parameters' comparison.

## 6.2 Discussion of the results

The discussion of the results obtained is based on the calculation of measurement errors between the developed device and the GIMA OXY-2 pulse oximeter. According to the tables and the graphs in the previous section, it is possible to calculate the absolute and the relative errors for the pulse rate and the absolute error for the arterial oxygen saturation. The acquisition of the values deals with a signal of 60-seconds. The fourteen acquired values for each parameter (PR and SpO<sub>2</sub>) are averaged for the developed device and the GIMA OXY-2. Based on the calculated average values, the errors are computed. The following table summarizes the obtained values of the errors for each subject.

Subject	$\epsilon_{a,PR}$ [bpm]	$\epsilon_{r,PR}$ [%]	$\epsilon_{a,SpO_2}$ [%]
1	1.20	1.80	-0.93
2	0.50	0.70	-0.21
3	0.29	0.49	0.79
4	0.14	0.19	1.80
5	1.64	2.15	1.71
6	0.28	0.44	1.43
7	0.36	0.42	1.5
8	0.43	0.58	1.07
9	0.78	0.94	0.78
10	0.10	0.10	-0.78
11	0.86	1.10	1.29
12	0.28	0.40	2.07

**Table 6.13:** Measurement errors.

From the analysis of the results, it can be stated that there are much more accurate values of pulse rate for the older age group ( $> 56$  years old). It is sufficient to see that the highest errors for pulsation are associated with subjects 1-5-11, aged between 24 and 37 years old. In particular, subject 5 has the highest error in PR with a difference between the designed device and the reference device of approximately 2bpm, i.e., a relative error slightly higher than 2%. Concerning arterial oxygen saturation, on the other hand, there are differences in average values ranging between -1%/+2%. In contrast to PR, there is no noticeable difference, in this case, depending on the various age groups.

The difference in this behavior for the pulse rate could be because the younger age group has a less regular heartbeat than the adult age group. Indeed, analyzing the graphs of the PR of subjects 5-7-8-10 and comparing them with those of 2-3-9

shows a significantly less constant horizontal trend in values for the first-mentioned subjects. In addition to the trend in the graphs, the PRV values are significant in explaining the variability of heartbeats between the different age groups. Indeed, the analysis of the subjects' results shows that the highest average values for PRV are those associated with subjects aged between 23 and 37 years old, with average values between 35-50 ms. For the older age group, the average PRV values are between 15-25 ms. Relatively to what is expressed in section 4.2.3, the variability of heartbeats decreases with age, but in reality, there are no fixed and predetermined reference values for all subjects [24]. In fact, this value also varies greatly depending on lifestyle, habits (smoking, alcohol consumption), and physical activity [24].

In conclusion, it should be noted that all subjects when the analysis was made had no particular health problems, except for subject 9, who had pneumonia in the past months. To better test the device, it is correct to experiment with subjects with lower saturation levels or bradycardia or tachycardia. This can be a future work or research for the next students of *Wearable devices* course.

### 6.3 Analysis of PPG waveform and large artery stiffness

As seen in the *figure 2.6* and section 2.3.2, the dicrotic notch and the systolic and diastolic peaks are critical physical characteristics of the signal from which specific information can be derived. The two peaks are the results of complex interactions between the left ventricle and the systemic circulation. The systolic peak of the waveform arises mainly from a forward-going pressure wave transmitted along a direct path from the left ventricle to the finger [27]. The diastolic peak occurs mainly from pressure waves transmitted along the aorta to small arteries in the lower body, from where they are then reflected back along the aorta as a wave that travels to the finger [27].

Since aging is accompanied by increased stiffness of large elastic arteries, this leads to an increase in pulse wave velocity (PWV). As determined by an elevated aortic PWV, premature arterial aging is recognized as a significant risk factor for ischaemic heart disease [27].

A study by Milleseu et al., in collaboration with various research departments in London, demonstrates that an index related to large artery stiffness (SI) derived from the digital volume pulse (DVP) can be calculated through a PPG signal. Indeed, the contour of the DVP is formed due to a complex interaction between the left ventricle and the systemic circulation [27]. They have demonstrated that the contour of the DVP contains similar information to that of the peripheral pressure pulse. For this reason, DVP and its two typical peaks exhibited (systolic and diastolic) are used to calculate the index SI. The difference in time  $\Delta T$  between

the two peaks can thus be used to infer the transit time taken for pressure to propagate along the aorta and large arteries to the significant sites of reflection in the lower body and back to the root of the subclavian artery [27]. This path length is unknown but can be assumed to be proportional to subject height ( $h$ ). Since PWV over a given path equals path length/transit time, SI is formulated as:

$$SI = \frac{h}{\Delta T} [m/s] \quad (6.1)$$

Even if it is not a direct measure for large artery stiffness, it is related to PWV in the aorta and large arteries and hence to the stiffness of these arteries.

Based on the cited study, the PPG signals of subjects 8-11-12 with ages 23-30-56 are compared to calculate SI values and demonstrate how they vary with age. The figures below show the three signals identifying the systolic and diastolic peaks for each selected subject.

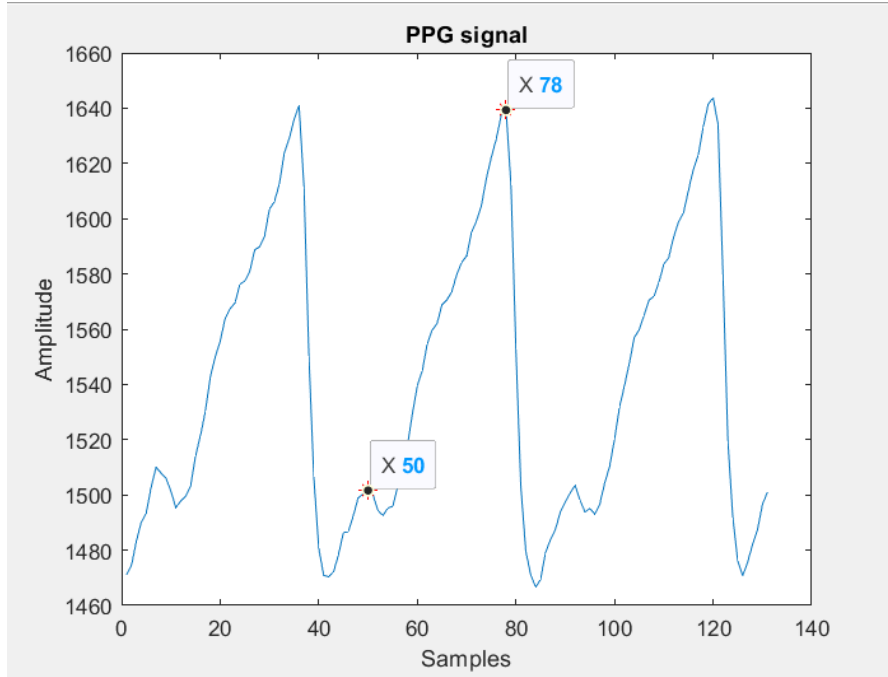


**Figure 6.13:** PPG signal of subject 8.

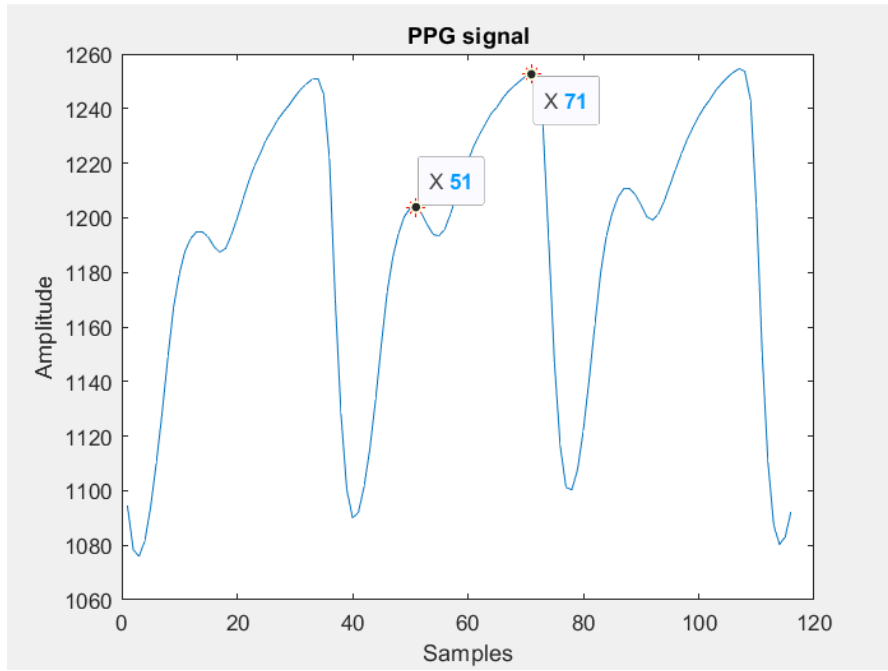


**Figure 6.14:** PPG signal of subject 11.

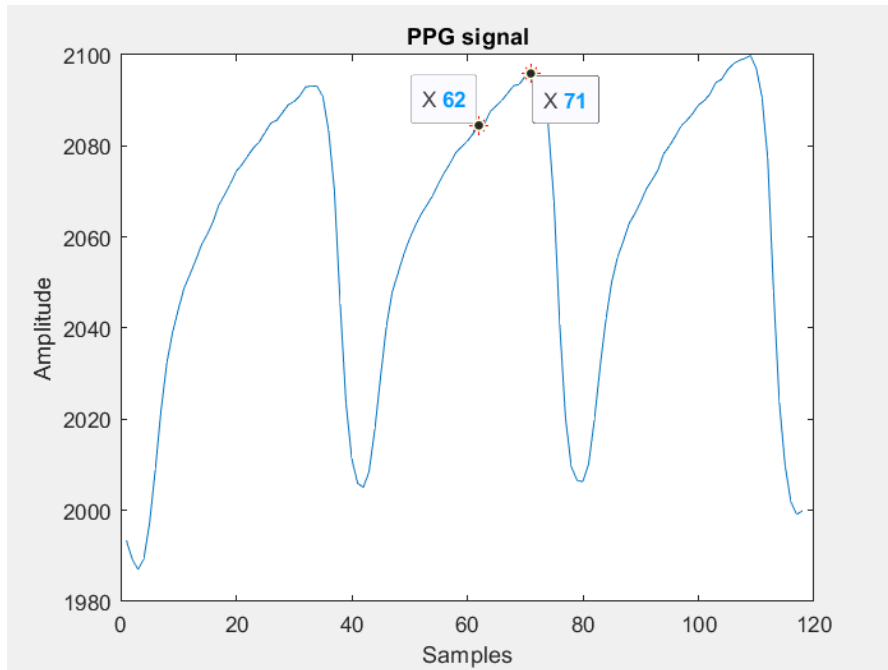


**Figure 6.15:** PPG signal of subject 12.

Through *equation* 6.1 it is possible to calculate SI values for the subjects. Table 6.14 resumes the obtained values.

Subject	Age [y]	Height [cm]	$\Delta T$ [ms]	SI [m/s]
<b>8</b>	23	170	560	<b>3.04</b>
<b>11</b>	30	183	400	<b>4.58</b>
<b>12</b>	56	176	180	<b>9.78</b>

**Table 6.14:** SI values.

Following the study cited above, it is shown that with increasing age, SI index values and thus PWV increase due to an increase in large artery stiffness. This behavior translates visually into a signal in which it is hardly possible to distinguish the dicrotic notch for subjects over 50/55 years of age. In contrast, it is much more visible for younger subjects.

## Chapter 7

# Conclusions and Future Work

This thesis project aims to create and test a finger transmittance pulse oximetry device. Before developing the electronic-circuit part, a careful and thorough study of the literature is made. Indeed, it is essential to understand the physical principles behind photoplethysmography, the characteristics of the PPG signal, the signal waveform, its frequency components, and the relative vital parameters that can be obtained.

Thanks to the research and the collaboration with Prof. J. Cosp, it was possible to carry out a circuit design that provides the correct signal acquisition using a photodiode and a dual-wavelength LED. Therefore, the clip realized by the laboratory technicians has two cavities for the appropriate insertion of the components mentioned above. The software part for correctly switching on the LEDs and acquiring the PPG signals is managed by the Arduino IDE software, using the C language. Once the signals are acquired, appropriate algorithms must be implemented to calculate the vital parameters. As described in Chapter 4, these algorithms are implemented in MATLAB as the graphic user interface that allows PPG signals to be displayed and the parameters to be read in real-time. The validation of the algorithms for vital parameters is done after verifying the correct signal acquisition. For proper verification and calibration of the device, it would have been necessary to use an ECG as a comparison instrument and a CO-oximeter for the R-SpO<sub>2</sub> calibration line. Without such tools, the used reference device is a standard GIMA OXY-2 pulse oximeter.

Some considerations and observations arise from the experimental tests carried out during the project. Firstly, it can be seen that if the pressure of the finger in the clip increases as if pressing it down on the desk, the signal decreases in intensity, and there is a significant distortion in the visualization. Furthermore,



when the ambient light is high, the correct reading of the parameters, as well as the display of the signal, is not possible for some patients. This problem is due to the high ambient light component that increases the current  $I_p$  flowing through the photodiode and so leads the OpAmps to saturate. A solution for this issue is to cover the clip with paper to shield the external light as much as possible. Moreover, for some subjects in the younger age group, there are sometimes reading errors with outsider values that are eliminated because they do not correspond to actual readings.

As for the web app, on the other hand, it was tested both with users connected on the same network and with users connected on different networks, even in different countries. For the web app to work correctly, it is necessary to have a strong and stable connection. Otherwise, it is sometimes impossible to display the signal in real-time. Furthermore, MATLAB Web Apps are not supported on mobile devices. Another limitation is that if the primary user who has to share the app is in a public environment where the router cannot be accessed to allow public connections, distant users cannot use the app. A final minor consideration concerns the 'HTTP' communication protocol used to share the app. HTTP is not a protocol with a security layer, such as password entry or user identification. Therefore, some data are at risk of being accessed by unwanted users.

Finally, by summarising the values obtained through the experimental tests, the device created has good accuracy compared with the reference device. Of course, many improvements can be made. Below are listed some proposals that could contribute to the improvement of the project:

- Developing a clip with a different shape that can completely dim the ambient light.
- Use more accurate reference instruments (such as ECG or CO-oximeter) for calibrating the device and calculating other vital parameters such as blood pressure.
- Use a lower sampling rate that can cut out network frequency components.
- Try to implement more the algorithms for calculating vital parameters to achieve even better results.
- Create a new GUI with other software and programming languages that are widely used in the field of engineering and biomedicine, such as Python.
- Use secure connections (SSL) using an HTTPS protocol to encrypt data transfer and protect it from external users.
- Development of an online database that healthcare providers can easily access.

Even though photoplethysmography has been used clinically in the last decades in pulse oximeters, there is still much opportunity to exploit the technology for further innovations. This is also thanks to the widespread use of wearable devices that help the prevention and the constant patient monitoring.

Lastly, an important aspect to emphasize and stress is the development of remote technologies such as apps or Bluetooth communications that align with the innovations of recent years in medicine. Indeed, there is an increasing move toward the world of telemedicine, which includes telemonitoring and telerehabilitation and beyond, to meet both the needs of the patient and facilitate the work of healthcare providers.

# Electric scheme and PCB

### A.0.1 Electric scheme

*Fig. A.1* depicts the electric scheme of the whole circuit and all the connections with the Arduino Due microcontroller.

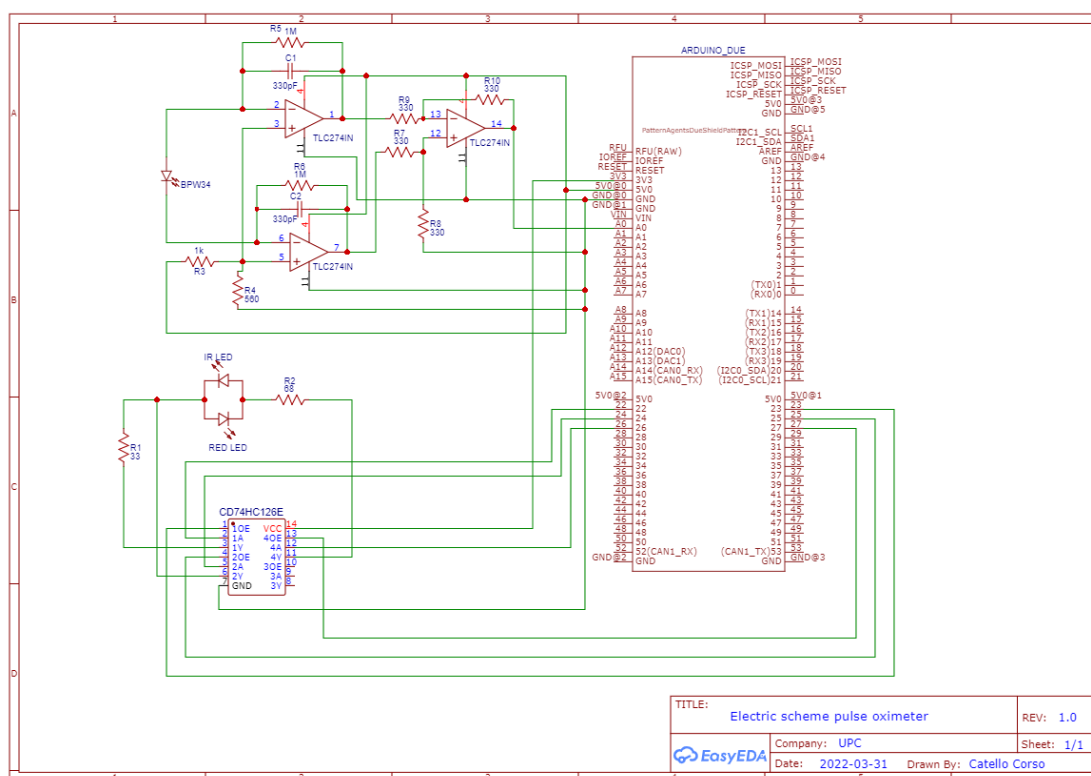


**Figure A.1:** Electric scheme.

### A.0.2 PCB manufacturing

The PCB design is carried out using *EasyEDA* software. The design involves the use of both layers (bottom and top) of the board.

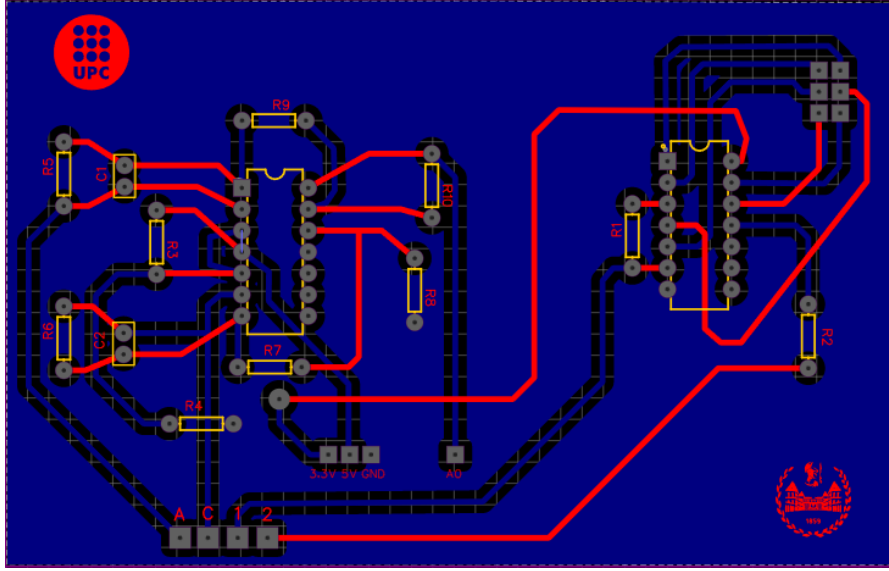


**Figure A.2:** PCB design in EasyEDA. [Scale 1:1]

As can be seen from the *fig.* A.2, the layer with the connections in blue represents the bottom layer in which there is a copper area to make the various connections to GND. On the other hand, the links made in red are those for the top layer. The top and the bottom layers designs are represented in the following figures.

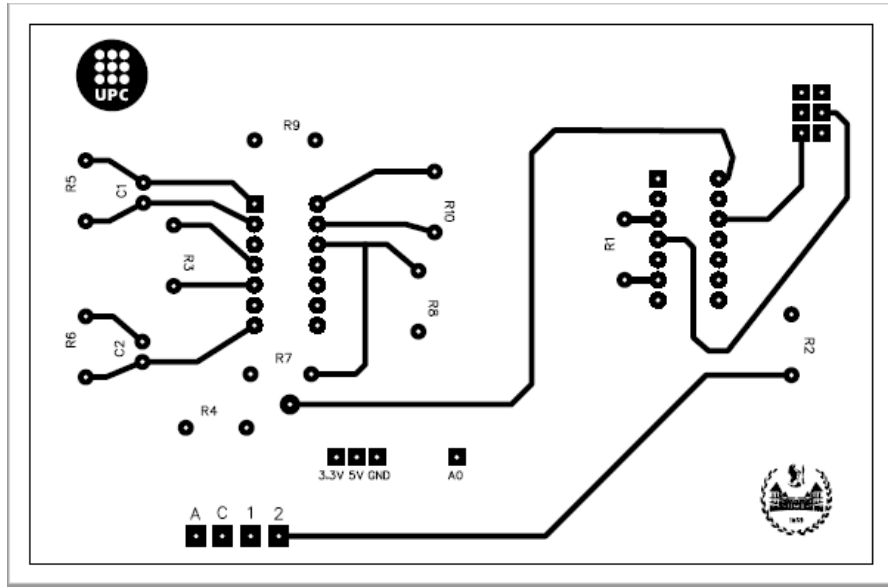


**Figure A.3:** Top Layer of PCB design. [Scale 1:1]

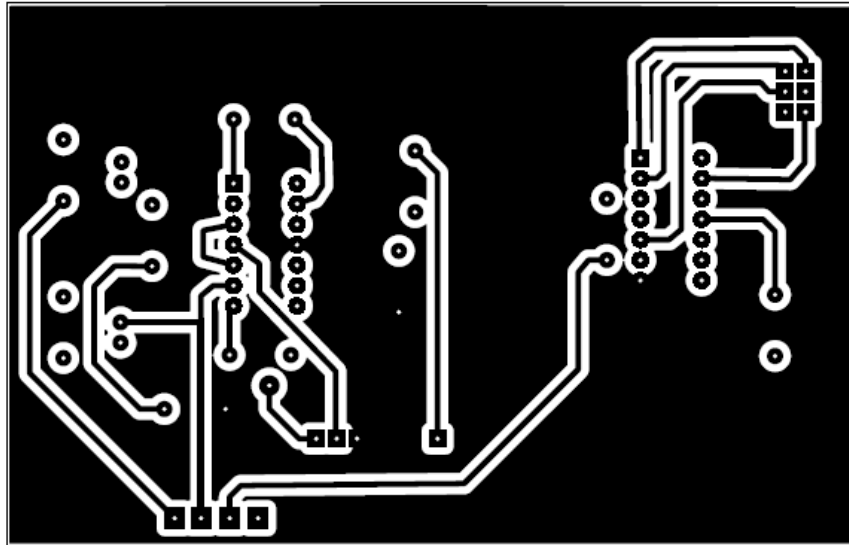
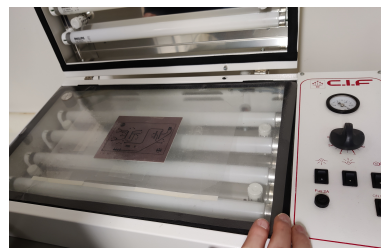


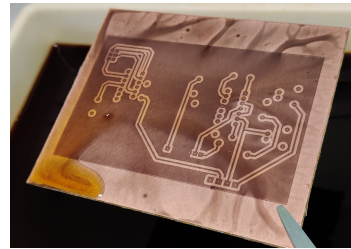
**Figure A.4:** Bottom Layer of PCB design. [Scale 1:1]

The four pads at the bottom left are used as inputs for the probe. On the other hand, the six pads on the top right and the other four pads relating to the power supply, GND, and the A0 pin are soldered to be plugged into the appropriate pins on the ARDUINO.

As far as the manufacturing process is concerned, a positive double-layer glass fiber plate is used. The two masks used to impress the circuit are printed on a transparent sheet and then overlapped. The board with the masks is placed in a UV vacuum machine for three minutes. UV exposure is used to impress the circuit onto the board. Afterward, the board is immersed in a solution of water and caustic soda to remove the photoresist on the board. It is then rinsed with water before the immersion in a 25%  $\text{H}_2\text{O}_2$ , 25%  $\text{HCl}$  and 50%  $\text{H}_2\text{O}$  solution. This last solution removes the excess copper. Finally, the last process involves cleaning the board with ethanol. The figures below show some steps of the manufacturing process.

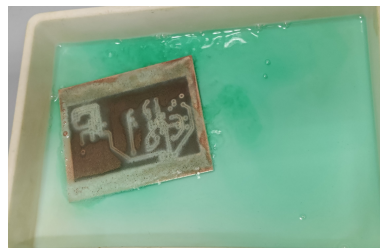


((a)) UV exposure.

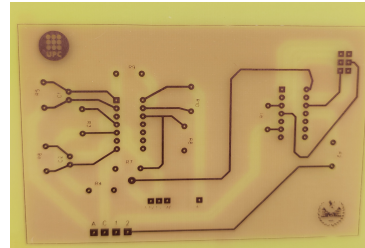


((b)) Immersion in  $\text{H}_2\text{O}$  and  $\text{NaOH}$  solution.

**Figure A.5:** Step 1-2 of PCB manufacturing.



((a)) Immersion in  $\text{H}_2\text{O}_2$ ,  $\text{HCl}$  and  $\text{H}_2\text{O}$  solution.



((b)) PCB after ethanol cleaning.

**Figure A.6:** Step 3-4 of PCB manufacturing.

In the end the holes are suitably drilled on the board to weld the components with tin solder.

## Appendix B

# MATLAB codes for vital parameters' algorithms

### B.0.1 Algorithm for PR calculation

```
function [pr] = pulserate_f(signal,c,ka,kb)

signal_f = filtfilt(kb,ka,signal(((c-1)*250+1): c*250));

[pmin,indmin] = findpeaks(-signal_f); % findpeaks to find all the minima
% relative and absolute
% in the range of 150 samples
mval = mean(signal_f); % calculate the mean value of the 250 samples range
t = 1;
j = 1;

for k= 1: length(pmin)
    if indmin(k) - 5 > 0
        if -pmin(k) < mval && signal_f(indmin(k)-5) > -pmin(k)

% 1st condition: if the minimum is < than the mean value is accepted
% 2nd condition: if the value of the signal at five samples before the one
% analyzed is higher than the minimum
% then it can be an absolute minimum

            index(t) = indmin(k); % set in the vector "index" the index
% of the minimum found

            if t == 1
                itsmin(j) = -pmin(k); % acquire the first absolute minimum
```

```

        itsind(j) = indmin(k);
        j = j+1;
    end

    if t > 1 && index(t)-index(t-1) > 15 % acquire the absolute minimum
        % if the difference of the index w.r.t
        % the previous minimum is > 15 samples ---> this means that is
        % an absolute minimum

        itsmin(j) = -pmin(k);
        itsind(j) = indmin(k) ;
        j = j+1;
    end

    t = t+1;
end
end
end

for z= 2 : length(itsind)

    val(z-1) = (3000/(itsind(z)-itsind(z-1))); % save in the vector "val"
    % the values of bpm for each cardiac cycle

end

pr = round(sum(val)/(length(itsind)-1)); % average value for heartrate in bpm

end

```



## B.0.2 Algorithm 1 for SpO<sub>2</sub> calculation

```
function [SpO2] = arterialO2saturation(signal1,signal2,c,ka,kb)

signal1_f = filtfilt(kb,ka,signal1(((c-1)*250+1): c*250+5));
signal2_f = filtfilt(kb,ka,signal2(((c-1)*250+1): c*250+5));
DC_R = mean(signal1(((c-1)*250+1): c*250+5));
DC_IR = mean(signal2(((c-1)*250+1): c*250+5));

%% Calculation of minima and maxima for Red signal
% Calculating minima of Red signal

[pminR,indminR] = findpeaks(-signal1_f(1:250)); % findpeaks to find all
% the minima relative and absolute
% in the range of 150 samples
mvalR = mean(signal1_f(1:250)); % calculate the mean value
% of the 150 samples range
t = 1;
j = 1;

for k= 1: length(pminR)
    if indminR(k) - 5 > 0
        if -pminR(k) < mvalR && signal1_f(indminR(k)-5) > -pminR(k)

            % 1st condition: if the minimum is < than the mean value is accepted
            % 2nd condition: if the value of the signal at five samples before the one
            % analyzed is higher than the minimum
            % then it can be an absolute minimum

            indexR(t) = indminR(k); % set in the vector "index" the index
            % of the minimum found + the samples shift

            if t == 1
                itsminR(j) = -pminR(k); % acquire the first absolute minimum
                itsindminR(j) = indminR(k);
                j = j+1;
            end

            if t > 1 && indexR(t)-indexR(t-1) > 15 % acquire the absolute minimum
                % if the different of the index w.r.t
                % the previous minimum is > 15 samples ---> this means that is
                % an absolute minimum

                itsminR(j) = -pminR(k);
                itsindminR(j) = indminR(k) ;
```

```

        j = j+1;
    end

    t = t+1;
end
end
end

% Calculating maxima for Red signal

[pmaxR,indmaxR] = findpeaks(signal1_f(1:250));
% DC_R = mean(signal1((c*250 -249): c*250)));
t = 1;
j = 1;
for k= 1: length(pmaxR)
    if pmaxR(k) > mvalR && signal1_f(indmaxR(k)+5) < mvalR

        indexR2(t) = indmaxR(k);

        if t == 1
            itsmaxR(j) = pmaxR(k);
            itsindmaxR(j) = indmaxR(k);
            j = j+1;
        end

        if t > 1 && indexR2(t)- itsindmaxR(j-1) > 15
            itsmaxR(j) = pmaxR(k);
            itsindmaxR(j) = indmaxR(k);
            j = j+1;
        end
        t = t+1;
    end
end

for y=1:min(length(itsindminR),length(itsindmaxR))

    AC_R(y) = itsmaxR(y)-itsminR(y);

end
AC_Ravg = sum(AC_R)/y;
ratio_Red = AC_Ravg/DC_R;

%% Calculation of minima and maxima for IR signal
% Calculating minima of IR signal

```

```

[pminIR,indminIR] = findpeaks(-signal2_f(1:250)); % findpeaks to find all
%the minima relative and absolute
% in the range of 150 samples
mvalIR = mean(signal2_f(1:250)); % calculate the mean value
% of the 150 samples range
t = 1;
j = 1;

for k= 1: length(pminIR)
    if indminIR(k) - 5 > 0
        if -pminIR(k) < mvalIR && signal2_f(indminIR(k)-5) > -pminIR(k)

            % 1st condition: if the minimum is < than the mean value is accepted
            % 2nd condition: if the value of the signal at five samples before the one
            % analyzed is higher than the minimum
            % then it can be an absolute minimum

            indexIR(t) = indminIR(k); % set in the vector "index" the index
            % of the minimum found

            if t == 1
                itsminIR(j) = -pminIR(k); % acquire the first absolute minimum
                itsindminIR(j) = indminIR(k);
                j = j+1;
            end

            if t > 1 && indexIR(t)-indexIR(t-1) > 15 % acquire the absolute minimum
                % if the different of the index w.r.t
                % the previous minimum is > 15 samples ---> this means that is
                % an absolute minimum

                itsminIR(j) = -pminIR(k);
                itsindminIR(j) = indminIR(k) ;
                j = j+1;
            end

            t = t+1;
        end
    end
end

% Calculating maxima for IR signal

[pmaxIR,indmaxIR] = findpeaks(signal2_f(1:250));

```

```

% DC_R = mean(signal1((c*250 -249): c*250)));
t = 1;
j = 1;
for k= 1: length(pmaxIR)
    if pmaxIR(k) > mvalIR && signal2_f(indmaxIR(k)+5) < mvalIR

        indexIR2(t) = indmaxIR(k);

        if t == 1
            itsmaxIR(j) = pmaxIR(k);
            itsindmaxIR(j) = indmaxIR(k);
            j = j+1;
        end

        if t > 1 && indexIR2(t)- itsindmaxIR(j-1) > 15
            itsmaxIR(j) = pmaxIR(k);
            itsindmaxIR(j) = indmaxIR(k);
            j = j+1;
        end
        t = t+1;
    end
end

for y=1:min(length(itsindminIR),length(itsindmaxIR))

    AC_IR(y) = itsmaxIR(y)-itsminIR(y);

end
AC_IRavg = sum(AC_IR)/y;
ratio_IR = AC_IRavg/DC_IR;

% Ratio of Ratio for calculating SpO2

RoR = ratio_Red/ratio_IR;
SpO2 = round(115.15 - RoR*28.619);

end

```

# Bibliography

- [1] *WHO Coronavirus (COVID-19) Dashboard / WHO Coronavirus (COVID-19) Dashboard With Vaccination Data*. URL: <https://covid19.who.int/>. (accessed: 02.03.2022) (cit. on p. 1).
- [2] J. G. Webster. *Design of pulse oximeters*. Institute of Physics Pub, 1997 (cit. on pp. 1, 3, 4, 6–10, 13, 19).
- [3] *Pulse Oximetry: Uses, Readings, and How It Works*. URL: <https://www.healthline.com/health/pulse-oximetry>. (accessed: 02.03.2022) (cit. on p. 3).
- [4] Amit Shah and Kirk Shelley. «Is pulse oximetry an essential tool or just another distraction? The role of the pulse oximeter in modern anesthesia care». In: *Journal of clinical monitoring and computing* 27 (Jan. 2013). DOI: 10.1007/s10877-013-9428-7 (cit. on p. 3).
- [5] *Oxygen saturation: normal values measurement - cosinuss°*. URL: <https://www.cosinuss.com/en/measured-data/vital-signs/oxygen-saturation/>. (accessed: 02.03.2022) (cit. on p. 4).
- [6] Amal Jubran. «Pulse oximetry». In: (1364). ISSN: 1364-8535. URL: <http://ccforum.com> (cit. on p. 4).
- [7] *Absorption spectra of deoxygenated Hb and oxygenated HbO<sub>2</sub> blood with... / Download Scientific Diagram*. URL: [https://www.researchgate.net/figure/Absorption-spectra-of-deoxygenated-Hb-and-oxygenated-HbO2-blood-with-the-isosbestic\\_fig4\\_46034130](https://www.researchgate.net/figure/Absorption-spectra-of-deoxygenated-Hb-and-oxygenated-HbO2-blood-with-the-isosbestic_fig4_46034130). (accessed: 25.05.2022) (cit. on p. 5).
- [8] Edward D. Chan, Michael M. Chan, and Mallory M. Chan. *Pulse oximetry: Understanding its basic principles facilitates appreciation of its limitations*. June 2013. DOI: 10.1016/j.rmed.2013.02.004 (cit. on pp. 5, 6, 9, 13).
- [9] *Principles of pulse oximetry / Deranged Physiology*. URL: <https://derangedphysiology.com/cicm-primary-exam/required-reading/respiratory-system/Chapter%20410/principles-pulse-oximetry>. (accessed: 02.03.2022) (cit. on pp. 10, 11).

- [10] Dennis J. McMahon. «6001759A-There's no such thing as a SpO2 simulator<sub>w</sub>». In: *Fluke Biomedical* (2013) (cit. on p. 10).
- [11] Mohamed Elgendi. *On the Analysis of Fingertip Photoplethysmogram Signals*. 2012, pp. 14–25 (cit. on pp. 11, 33).
- [12] Stephen A Esper, Assistant Professor of Anesthesiology, Michael R Pinsky, Professor of Critical Care Medicine, and Cardiovascular Diseases. «Arterial waveform analysis». In: *Best Practice Research Clinical Anaesthesiology* 28 (2014), pp. 363–380. DOI: 10.1016/j.bpa.2014.08.002. URL: <http://dx.doi.org/10.1016/j.bpa.2014.08.0021521-6896/> (cit. on p. 11).
- [13] *Using Reflectometry for a PPG Waveform*. URL: <https://www.maximintegrated.com/en/design/technical-documents/app-notes/6/6547.html>. (accessed: 02.03.2022) (cit. on p. 11).
- [14] Fred Shaffer and J. P. Ginsberg. *An Overview of Heart Rate Variability Metrics and Norms*. Sept. 2017. DOI: 10.3389/fpubh.2017.00258 (cit. on p. 12).
- [15] Hangsik Shin. «Ambient temperature effect on pulse rate variability as an alternative to heart rate variability in young adult». In: *Journal of Clinical Monitoring and Computing* 30 (6 Dec. 2016), pp. 939–948. ISSN: 15732614. DOI: 10.1007/s10877-015-9798-0 (cit. on p. 12).
- [16] *Pulse transit time: an appraisal of potential clinical applications | Thorax*. URL: <https://thorax.bmj.com/content/54/5/452>. (accessed: 02.03.2022) (cit. on p. 12).
- [17] Susan DeMeulenaere. «Pulse Oximetry: Uses and Limitations». In: *The Journal for Nurse Practitioners* 3 (5 May 2007), pp. 312–317. ISSN: 1555-4155. DOI: 10.1016/J.NURPRA.2007.02.021. URL: [http://www.npjjournal.org/article/S1555415507002103/fulltext%20http://www.npjjournal.org/article/S1555415507002103/abstract%20https://www.npjjournal.org/article/S1555-4155\(07\)00210-3/abstract](http://www.npjjournal.org/article/S1555415507002103/fulltext%20http://www.npjjournal.org/article/S1555415507002103/abstract%20https://www.npjjournal.org/article/S1555-4155(07)00210-3/abstract) (cit. on p. 13).
- [18] Frain and Megan. *Sensor solutions /// Meas emitter assembly ELM-4000 series*. 2018 (cit. on pp. 14, 22).
- [19] Vishay Intertechnology, *Datasheet: Silicon PIN Photodiode*. URL: [www.vishay.com/doc?91000](http://www.vishay.com/doc?91000) (cit. on p. 14).
- [20] Praveen Aroul. *Getting Started Guide Miniaturized Pulse Oximeter Reference Design* (cit. on p. 20).

- [21] *CETRONIC :: Detalle del producto*. URL: [https://www.cetronic.es/sqlcommerce/disenos/plantilla1/seccion/producto/DetalleProducto.jsp?idIdioma=&idTienda=93&codProducto=82-BPW34&cPath=1210&gclid=Cj0KCQjw-pCVBhCFARIsAGMxhAebWKRCRKCXdThqAljcadwHEntqjlZHW7XXFJRb4NntyAEPb6se0JcaAvZWEALw\\_wcB](https://www.cetronic.es/sqlcommerce/disenos/plantilla1/seccion/producto/DetalleProducto.jsp?idIdioma=&idTienda=93&codProducto=82-BPW34&cPath=1210&gclid=Cj0KCQjw-pCVBhCFARIsAGMxhAebWKRCRKCXdThqAljcadwHEntqjlZHW7XXFJRb4NntyAEPb6se0JcaAvZWEALw_wcB). (accessed: 11.06.2022) (cit. on p. 22).
- [22] Peter H. Charlton, Panicos A. Kyriacou, Jonathan Mant, Vaidotas Marozas, Phil Chowienczyk, and Jordi Alastruey. «Wearable Photoplethysmography for Cardiovascular Monitoring». In: *Proceedings of the IEEE* 110 (3 Mar. 2022), pp. 355–381. ISSN: 0018-9219. DOI: 10.1109/jproc.2022.3149785 (cit. on pp. 31, 35, 39).
- [23] *Renesas Technology, Datasheet: Pulse Oximeter Algorithm for SpO2, Heart Rate, and Respiration Rate Application Note*. 2021 (cit. on p. 35).
- [24] *What is a Good HRV? / Heart Rate Variability / WHOOP*. URL: <https://www.whoop.com/thelocker/what-is-a-good-hrv/>. (accessed: 27.05.2022) (cit. on pp. 40, 77).
- [25] *Which Finger You Should Use a Pulse Oximeter On / CMI Health*. URL: <https://www.cmihealth.com/blogs/news/which-finger-you-should-use-a-pulse-oximeter-on>. (accessed: 31.05.2022) (cit. on pp. 42, 44).
- [26] *Private vs. Public IP Addresses / Differences Explained / Avast*. URL: <https://www.avast.com/c-ip-address-public-vs-private>. (accessed: 08.06.2022) (cit. on pp. 48, 49).
- [27] S C Millasseau, R P Kelly, J M Ritter, and P J Chowienczyk. *A B S T R A C T*. 2002, pp. 371–377 (cit. on pp. 77, 78).





# Acknowledgements

Il **2 Ottobre 2017** muovevo i primi passi nel mondo universitario, una data indimenticabile per esperienze e sentimenti. Impossibile cancellare dalla memoria il battito accelerato del mio cuore per il mix di emozioni che quel giorno mi travolgevano: insicurezza e preoccupazione per il nuovo contesto in cui ero in procinto di proiettarci, commozione per il distacco dall'ambiente familiare, ansia per la consapevolezza del nuovo percorso di vita che avrei dovuto sperimentare facendo leva solo sulle mie forze e capacità.

Il **14 Dicembre 2022**, dopo un quinquennio che mi ha fatto crescere sia didatticamente sia come persona umana, il mio percorso giunge al termine.

E' stato un tragitto faticoso, non privo di difficoltà esperienziali e formative ma anche ricco di soddisfazioni e di gratificazioni in cui mi sono messo alla prova con serietà e costanza di impegno, sempre con tenacia, senso di responsabilità e spirito di sacrificio per non mollare. Tanto più le mie ore di studio aumentavano quanto più le difficoltà crescevano rendendo ardua la meta. E sono innumerevoli le ore di studio che richiede questa facoltà!

Finalmente, con gioia e consapevolezza, sono giunto all'ambito traguardo ma non come protagonista unico. Sono grato e ringrazio soprattutto il professor Vallan che con professionalità e disponibilità è sempre stato un sicuro riferimento; non si è risparmiato in consigli e chiarimenti, con apertura e gentilezza, nel periodo di stesura della tesi, nonostante la distanza.

Gracias al profesor Jordi Cosp por su paciencia, profesionalidad y cooperación, que fueron esenciales para la redacción de este proyecto de tesis. Gracias a los técnicos de laboratorio Francesc, Fernando y Alfonso, que siempre fueron amables en ayudarme.

Grande sostegno ho ricevuto dalla mia famiglia, presenza forte e costante nella mia vita. Gli obiettivi conseguiti non sarebbero stati possibili se non avessi potuto contare su i miei cari che hanno scommesso su di me sostenendomi e incoraggiandomi sempre. Ringrazio i miei genitori per la fiducia, l'affetto e le spese che hanno dovuto sostenere per i miei studi. Mio padre, mia madre, mio fratello sono il bene più prezioso che possiedo. Custodirò il loro amore per sempre e cercherò di non deluderli mai. Il mio lavoro di tesi, portato a termine con determinazione ed impegno lo

dedico a loro che sono stati la mia forza.

Un pensiero di affetto e gratitudine rivolgo poi ad una persona molto cara che ho avuto paura di perdere, vivendo giorni difficili di grande ansia, lontano da casa, pur essendogli vicino con il cuore. Grazie a Dio, caro zio Pino, ora puoi condividere la mia felicità. Ti ringrazio per quanto hai fatto e fai per me.

Grazie anche ai miei zii ed ai cugini per la loro costante vicinanza con telefonate, messaggi e preghiere che non mi hanno mai fatto sentire solo.

Non posso poi dimenticare i miei compagni e colleghi universitari per i consigli e il supporto dati nei momenti di difficoltà. Sono grato a Martina e Silvia per l'aiuto didattico e la cordialità nei rapporti interpersonali. Dal loro coraggio nell'affrontare e risolvere le situazioni della vita, ho attinto forza e motivazione. Grazie, amiche mie, per quanto avete fatto per me! Senza di voi gran parte di questo percorso biennale sarebbe stato in salita. Sono onorato di avervi come amiche e colleghe.

Un grazie di cuore va a tutti i miei amici che sin dall'infanzia mi sono stati vicino seguendomi ovunque andassi. Con loro ho condiviso momenti indimenticabili. La loro allegria, la spensieratezza, la leggerezza sono state fondamentali per farmi distrarre e prendere una pausa dallo studio quando necessario. Non esiste distanza che ci separi; il nostro rapporto resterà invariato. So di poter contare sempre su di voi.

Ancora un grazie per il mio amico Antonio con cui ho vissuto dieci mesi stupendi a Barcellona. Leale e affabile, sempre pronto ad aiutarmi, a consigliarmi e a condividere i momenti della mia vita. Grazie per aver creduto in me, per avermi spronato a proseguire questo percorso di tesi. Ti auguro il meglio che la vita possa riservarti.

Ringrazio ancora una volta i ragazzi di via Polonghera che mi hanno accompagnato per gran parte del mio percorso di studi. Siete stati la mia famiglia torinese.

Grazie a Carmelo e Valentina per la loro ospitalità, disponibilità e vicinanza nei dieci mesi vissuti all'estero. Mi avete fatto sentire a casa e voluto bene.

I thank my roommates in Barcelona, especially Alaa and Lucas. Amazing guys, always available and ready to help me. Living with you has been a pleasure and a reason to get to know different cultures in depth. I wish you all the best for the future.

Infine, ringrazio i miei nonni che dall'alto mi proteggono e spero che la vita mi conceda le opportunità per realizzare i miei sogni.

